Zircon U-Pb Age Constraints on the Exhumation of the Lesser Himalayas from the Laxmi Basin, Arabian Sea

Peng Zhou[1,2], Daniel F. Stockli[3], Thomas Ireland[4], Richard W. Murray[5], Peter D. Clift[1]

[1] Department of Geology and Geophysics, Louisiana State University, Baton Rouge, LA 70803, USA

[2]Department of Physics, Geology, and Engineering Technology, Northern Kentucky University, Highland Heights, KY 41099, USA

[3] Department of Geological Sciences, Jackson School of Geosciences, University of Texas, Austin, TX 78712-1722, USA

[4] Department of Earth and Environment, Boston University, Boston, MA 02215, USA

[5] Woods Hole Oceanographic Institution, Woods Hole, MA 02543, USA

Corresponding author: Peter Clift (pclift@lsu.edu)

Key Points:

- First basin-wide study of how regional erosion patterns have changed through time since 15.5 Ma in the Western Himalaya and Karakoram.
- Geochemical and geochronological analyses show increased relative erosion from the Himalaya compared to the Karakoram at 7.99–7.78 Ma.
- Changing patterns of erosion correlate with climatic drying at ~7.7–6.3 Ma, and relate to solid Earth tectonic forces building topography.

Abstract

The Indus Fan, located in the Arabian Sea, contains the bulk of the sediment eroded from the Western Himalaya and Karakoram. Scientific drilling in the Laxmi Basin by the International Ocean Discovery Program (IODP) provides an erosional record from the Indus River drainage dating back to 10.8 Ma, and with a single sample from 15.5 Ma. We dated detrital zircon grains by U-Pb geochronology to reconstruct how erosion patterns changed through time. Long-term increases in detrital zircon U-Pb components of 750–1200 Ma and 1500–2300 Ma show increasing preferential erosion of the Himalaya relative to the Karakoram at 7.99–7.78 Ma and more consistently starting by 5.87 Ma. An increase in the contribution of 1500–2300 Ma zircons starting by 1.56 Ma indicates significant unroofing of the Inner Lesser Himalaya (ILH) by that time. The trend in zircon U-Pb age populations is consistent with bulk sediment Nd isotope data implies greater zircon fertility in Himalayan bedrock compared to the Karakoram and Transhimalaya. The initial change in spatial erosion patterns at 7.0–5.87 Ma occurred during a time of drying climate in the Indus foreland. The increase in ILH erosion postdates the onset of dry-wet glacial-interglacial cycles suggesting some role for climate control. However, erosion driven by rising topography in response to formation of the Lesser Himalayan thrust duplex, especially during the Pliocene may also be important. The influence of the Nanga Parbat Massif to the bulk sediment flux is modest, in contrast to the situation in the eastern Himalaya syntaxis.

Keywords: Erosion, zircon, monsoon, Himalaya.

1 Introduction

Collision between India and Eurasia, starting about 50–60 Ma [*Garzanti et al.*, 1987; *Jaeger et al.*, 1989; *Klootwijk et al.*, 1992; *Najman et al.*, 2010], has resulted in the formation the largest mountain ranges on Earth. The timing of collision remains controversial but is best addressed by consideration of the stratigraphic record that shows the onset of mixed Indian-Eurasian sediments. Sedimentary rocks in the central and eastern Himalaya imply initial collision at 59 ± 1 Ma [*Hu et al.*, 2016]. Recent work combining Hf isotopes with U-Pb ages in zircon grains from the Tethyan Himalaya now show that sediment eroded from Eurasia, rather than oceanic island arcs, was reaching NW India by 54 Ma, requiring India-Eurasia collision before than time [*Najman et al.*, 2017]. The Himalaya have continued to evolve both in topography and structure as a result of ongoing tectonic deformation coupled with erosion, largely modulated by the strength of summer monsoon rains [*Bookhagen et al.*, 2005; *Clift et al.*, 2008b; *Wobus et al.*, 2003]. Sediments eroded from the Western Himalaya has been deposited in the Arabian Sea where they form the second largest sediment body on Earth, the Indus submarine fan [*Clift et al.*, 2001; *Kolla and Coumes*, 1987].

The sedimentary deposits of the Indus submarine fan represent an archive of the erosion and weathering processes in the Western Himalaya since the onset of continental collision, at least since ~45 Ma [*Clift et al.*, 2001]. While bedrocks exposed at the surface in the mountains can be used to reconstruct the uplift and exhumation of those particular rock formations, the submarine fan sedimentary record captures spatial and temporal variations of the long-term history of denudation, albeit one buffered by sediment transport processes. Because older portions of bedrocks have been completely removed by erosion and their exhumation history no

longer accessible, the sedimentary record becomes the only record of the earlier erosion and exhumation history. Although this record is partially available in the Himalayan foreland basin, these proximal, continental syn-tectonic deposits are more difficult to date at high resolution, and the sequence is truncated by significant unconformities, and deformed by progressive incorporation into the sub-Himalayan fold and thrust belt [*Najman*, 2006]. Moreover, any given section in the accreted foreland basin can only represent the sediment deposited from paleo-rivers that once flowed in front of the mountains in that region. As such a given section would preserve a history of erosion in a limited catchment of a particular part of the mountains, but does not provide a more integrated orogen-scale overview.

Sediments from the western Himalaya are delivered to the Arabian Sea by the Indus River and its eastern tributaries in the Punjab (Fig. 1A). The Indus is particularly sensitive to variations in the strength of the Asian monsoon because it lies on the western edge of the zone affected by this climatic phenomenon. As a result, variations in monsoon strength can have a major impact on both patterns and rates of erosion in the various ranges that comprise the western end of the Himalayan mountain chain (Fig. 1B). A number of studies have suggested that changes in monsoon intensity have significantly impacted the erosion history of the western Himalaya [*Bookhagen et al.*, 2005; *Clift et al.*, 2008a; *Clift et al.*, 2008b].

Debate continues regarding what controls the erosion of the Himalaya, with some workers favoring tectonic processes that drive rock uplift [*Burbank et al.*, 2003], as being the critical control, while others have argued for a dominance by monsoon rainfall and/or glaciation [*Whipple*, 2009; *Wobus et al.*, 2003]. These focus the sediment producing regions across a relatively narrow band of the range front and in turn drive exhumation of deep buried rocks [*Thiede et al.*, 2004]. It is however known that the erosion of the Himalaya is sensitive to climate change because sediment supply during and shortly after the Last Glacial Maximum (LGM) was preferentially focused in the Karakoram, while the strongest erosion has shifted into the Lesser Himalaya since the onset of the Holocene [*Clift et al.*, 2008a].

In this study we focus on the Late Miocene-Recent history and examine evidence for coupling between the tectonic evolution and the changing strength of summer monsoon rains. We take advantage of recently recovered sediments collected by the International Ocean Discovery Program (IODP) in 2015 from the Eastern Arabian Sea, which provide a record of erosion extending back to ~10.8 Ma, with one sample dated at ~15.5 Ma [*Pandey et al.*, 2016d]. An earlier lower-resolution study using detrital zircon grains and numerous bulk sediment Nd and Sr isotopes argued that changes in erosion across the Indus Basin were unconnected to climate change and largely manifest as increasing erosion of the Lesser Himalaya, especially starting at 1.9 Ma [*Clift et al.*, 2019b]. We test this model using an expanded set of new U-Pb ages from detrital zircon sand grains (1882 new ages from 15 additional samples, compared to 1335 ages from ten samples in the earlier work) coupled with a more sophisticated statistical treatment of the total data set in order to reconstruct the evolving patterns of erosion.

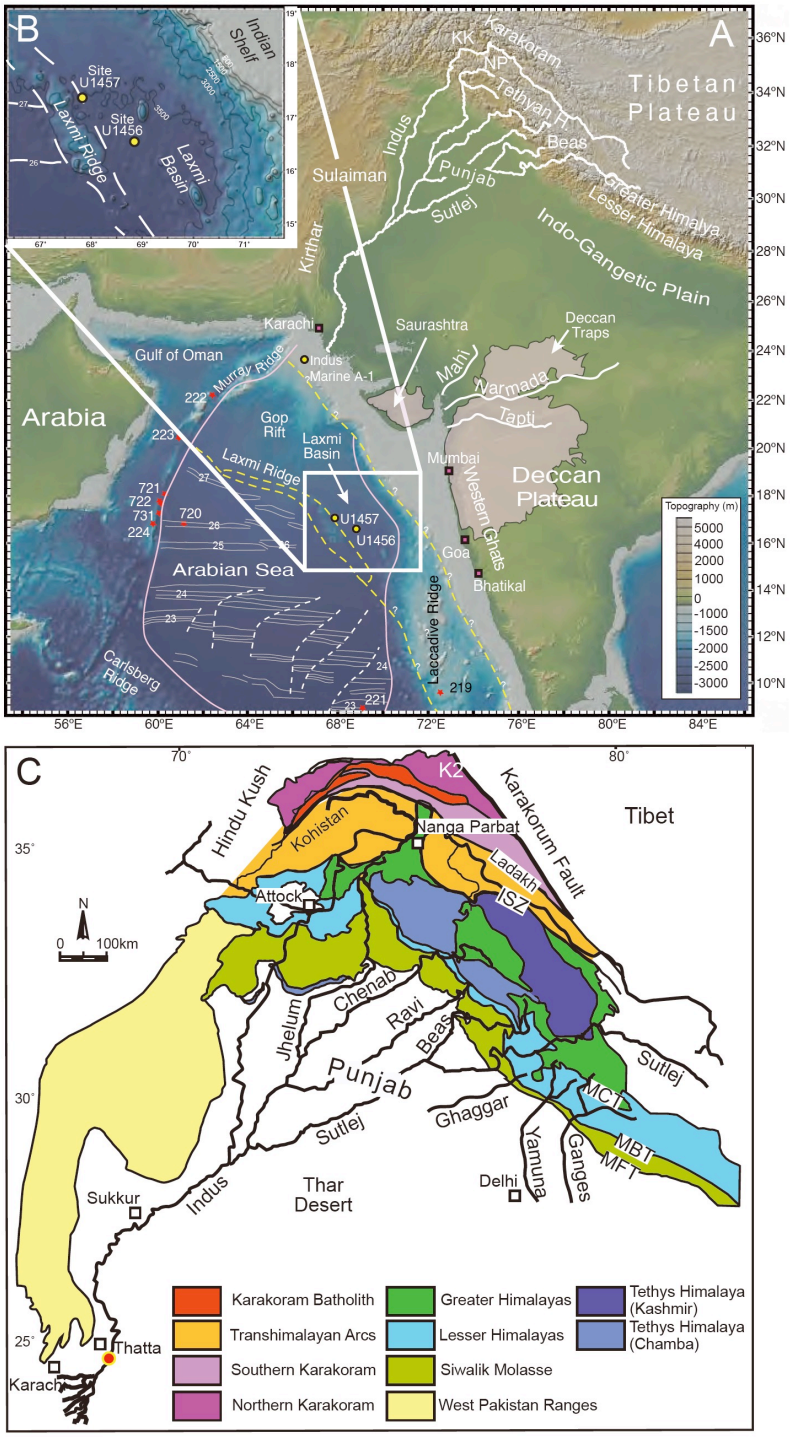

Figure 1. A) Shaded bathymetric and topographic map of the Arabian Sea and surrounding area showing the location of the drilling sites considered by this study. Map also shows the major tributary systems of the Indus River, as well as smaller peninsular India rivers and their source mountains. B) Inset map shows detail of the Laxmi Basin and location of the drill sites considered in this study. Numbered red circles indicate existing scientific boreholes from Deep Sea Drilling Project (DSDP) and Ocean Drilling Program (ODP). KK = Karakoram; NP = Nanga

Parbat. C) Geological map of the western Himalaya showing the major tectonic units that are eroded by the Indus River and its tributaries. Map is modified after Garzanti *et al.* [2005]. Rivers as shown in thick black lines. ISZ = Indus Suture Zone, MCT = Main Central Thrust, MBT = Main Boundary Thrust and MFT = Main Frontal Thrust. Thick black line shows the boundary of the Indus drainage, while thinner lines demark the limits of the major Himalayan tributaries. Figure is modified from Clift *et al.* [2019b].

2 Geologic Setting

The sediments analyzed in this study were retrieved from the Laxmi Basin in the Eastern Arabian Sea (Fig. 1A and 1B). This basin is separated from the rest of the Arabian Sea by a continental block known as Laxmi Ridge [*Pandey et al.*, 1995]. Rifting in Laxmi Basin preceded the breakup of the main Arabian basin, west of Laxmi Ridge, and likely occurred in the latest Cretaceous [*Bhattacharya et al.*, 1994]. Since that time 2–3 km of sediment have accumulated in the Laxmi Basin. Initial provenance investigation of these sediments using Nd isotopes and limited zircon U-Pb dating indicates that while some fine-grained material might be derived in from peninsular India, immediately to the east of the Laxmi Basin, most of the sediment was sourced from the Indus Delta, located around 800 km towards the north [*Clift et al.*, 2019b]. Continuous sedimentation in Laxmi Basin was interrupted by the emplacement of a large mass transport complex (MTC) just before 10.8 Ma, which eroded most of the Middle Miocene at Site U1456 [*Calvès et al.*, 2015; *Dailey et al.*, 2019]. At Site U1457 the MTC removed almost the entire sediment fill from the edge of Laxmi Ridge leaving only a thin deposit of red Paleocene mudstones [*Pandey et al.*, 2016b].

We also compare our sediments with those recovered as drill cuttings from the industrial borehole Indus Marine A-1 located on the Indus shelf (Fig. 1A). Because Indus Marine A-1 is located close to the Indus River mouth the source of sediment is more straight forward, and cannot have involved influence from the Indian Peninsula, as might be the case in the Laxmi Basin. This site penetrated into the Middle Miocene [*Shuaib*, 1982] and drill cuttings have been used to look at the evolving provenance using Nd isotope methods, going back further in time than possible at the IODP sites [*Clift and Blusztajn*, 2005; *Clift et al.*, 2019b]. The Indus Marine A-1 drill site is located on the relatively flat continental shelf and is only affected by growth faulting, but has otherwise escaped major tectonic deformation since the breakup of the Arabian Sea, except along its western edge adjacent to the Murray Ridge [*Clift et al.*, 2002a; *Gaedicke et al.*, 2002]. Unfortunately, the recovered sediments from Indus Marine A-1 are fine-grained and are not conducive to detrital zircon U-Pb dating in this proximal area. We examined the major element chemistry of the sediments at Indus Marine A-1 for comparison with the more distal drill sites sampled by IODP in order to demonstrate their Indus provenance. Neodymium isotope data indicate that Indus Marine A-1 sediments were derived from the Indus River, consistent with their proximal location, providing a useful comparison with the deep-water materials [*Clift and Blusztajn*, 2005].

Determining the provenance of the sediment delivered to the Arabian Sea is facilitated by the leverage of the significant spatial diversity of bedrock ages and lithologies within the Indus

drainage basin [*Hodges*, 2000; *Searle*, 1996]. Geochemical and isotopic differences between bedrock sources are transferred to the eroded sediment and although grains may be altered during the transport process, many of these differences are preserved in the final deposited sediment, allowing us to deconvolve the sources and variations using appropriate proxies. Figure 1C shows the various mountain ranges that comprise the main distinct source regions to the modern Indus River, including the Greater and Lesser Himalaya, the Tethyan Himalaya that lie further north, and that represent the telescoped, passive continental margin of Greater India [*Garzanti et al.*, 1987]. This unit is separated by the Indus Suture Zone from magmatic arc rocks of the Transhimalaya and Kohistan (Fig. 1C) that were largely emplaced in the Cretaceous and Paleogene [*Khan et al.*, 1997; *Rolland et al.*, 2002]. Further north, across the Shyok Suture Zone, lie the Karakoram, the old active margin of continental Eurasia, which also comprises Mesozoic arc rocks, and experienced magmatism after India-Euasia collision, most notably in the form of the Early Miocene Karakoram Batholith [*Ravikant et al.*, 2009; *Searle et al.*, 1989]. The Karakoram region was uplifted in response to both compressional tectonics and strike-slip displacement on the Karakoram Fault [*Searle and Phillips*, 2007]. Farther to the west the Hindu Kush mountains are characterized by a similar pre-collisional history as the Karakoram, but subsequently did not experience such dramatic or rapid unroofing [*Hildebrand et al.*, 2001; *Zhuang et al.*, 2018]. In addition, the Western Syntaxis of the mountain chain is marked by the Nanga Parbat Massif (Fig. 1C), characterized by high-grade metamorphic and igneous intrusive rocks that experienced recent, very rapid exhumation [*Zeitler et al.*, 1989]. However, it is unclear exactly when this process began because the rocks now at the surface are very young. Nonetheless, this does not preclude an earlier onset to erosion [*Chirouze et al.*, 2015].

The Greater Himalaya were emplaced along the Main Central Thrust (MCT) after ~24 Ma, placing them over the Lesser Himalaya [*Catlos et al.*, 2001; *Stephenson et al.*, 2001]. These in turn were unroofed and brought to the surface due to motion along the Main Boundary Thrust (MBT) and associated thrust duplexing [*Bollinger et al.*, 2004; *Huyghe et al.*, 2001]. Evidence from the Siwalik Group foreland basin sedimentary strata indicates that the Lesser Himalaya were exposed locally only after 9 Ma and more widely after 6 Ma in NW India [*Najman et al.*, 2009], although the Nd isotopes at Sites U1456 and U1457 imply that widespread unroofing of the Inner (Crystalline) Lesser Himalaya only began at 1.9 Ma [*Clift et al.*, 2019b]. The Siwalik Group rocks themselves have been up-thrusted and are presently eroding, recycling older sediments back into the river system. However, estimates derived from the incision of terraces in the Nepalese frontal Himalaya suggest that the Siwaliks contribute no more than about 15% of the total flux [*Lavé and Avouac*, 2000]. The western edge of the Indus drainage basin is characterized by fold and thrust belts (Sulaiman and Kirthar ranges, Fig. 1A), similar to the Siwalik Group in character [*Roddaz et al.*, 2011], but experiencing a more arid climate. Nonetheless, this environment need not limit erosion rates because of the strong erosion associated with occasional flash flooding events in vegetation-poor settings [*Molnar*, 2001], although study of heavy minerals in rivers draining these ranges and the lower Indus indicate that their contribution to the net sediment load is minor [*Garzanti et al.*, 2020].

Other potential sources of sediment delivered into the Laxmi Basin include the Precambrian cratonic rocks of peninsular India and associated Gondwanan sedimentary sequences [*Mukhopadhyay et al.*, 2010; *Yin et al.*, 2010], characterized by old (>500 Ma) bedrock zircon U-Pb ages, similar to those observed in the Himalaya, especially the Lesser

Himalaya. Zircon U-Pb dating, given its high closure temperature [*Hodges*, 2003], only records the initial crystallization or high-temperature metamorphism, and thus, does not allow us to exclude such old grains as having been derived from peninsular India rather than the Himalaya. Sediments eroded from the Deccan Plateau, the latest Cretaceous flood basalt province that dominates the Western Ghats, immediately onshore from the drilling area, were erupted around 65 Ma [*Courtillot et al.*, 2000] over a relatively short period of time. While these would be very distinctive, basalt is characterized by a very low zircon fertility and might not provide significant zircon grains of that age into the adjoining basin. Nd and Sr isotopic evidence suggests enhanced flux in muddy sediments to the Laxmi Basin during interglacial times [*Khim et al.*, 2019]. Low-resolution apatite fission track and zircon U-Pb studies have so far identified just a single sand at the IODP drill sites that was derived from the Indian peninsula [*Zhou et al.*, 2019].

3 Sedimentology and Stratigraphy

Drilling at Sites U1456 and U1457 penetrated ~1100 m below the seafloor in both locations, with the basement being reached at Site U1457 (Fig. 2)[*Pandey et al.*, 2016b]. Drilling at Site U1456 only just penetrated through the MTC, allowing a very short core of Middle Miocene sandstone to be recovered [*Pandey et al.*, 2016a]. Age assignments at both sites are made by combining biostratigraphy and magnetostratigraphy and we follow the age model of Pandey *et al.* [2016a] for Site U1456 and Pandey *et al.* [2016b] for Site U1457 (Fig. 2), with updates from Routledge *et al.* [2019]. Ages of individual samples are calculated assuming linear sedimentation between the dated points. At Site U1456 the sediments are relatively mud-rich, but with a number of silt and fine sand turbidite interbeds at 460–730 mbsf (meters below seafloor; Fig. 2A), which are overlain by a sequence of mud and carbonate-rich sediments. A thick, sand-rich package was recovered between 360 and 140 mbsf and interpreted as a submarine fan lobe [*Pandey et al.*, 2016a]. Above this sand-rich package, the section is dominated by mud and carbonate, interpreted as the product of hemipelagic sedimentation. Site U1457 is characterized by much lower proportions of sand, reflecting the drilling location on the flanks of the Laxmi Ridge. However, a sand-rich interval between 670 and 810 mbsf is overlain by a carbonate and mud-rich interval between 600 and 670 mbsf. More sand-rich beds were encountered between 470 and 600 mbsf. As at Site U1456, sediments shallower than 200 mbsf at Site U1457, are mud and carbonate-rich (Fig. 2). The coarse-grained intervals are again interpreted as lobe deposits [*Pandey et al.*, 2016b]. The sandy sediments are interpreted to be deposited by turbidity currents, with the muddy sediments representing hemipelagic intervals between depositional events. Changes in grain size might be driven by changes in the erosional power in the source regions, the discharge stream power of the river, or by changes in sea level, but could also reflect avulsion in the main depositional lobes in and out of Laxmi Basin and the main part of the Arabian Sea towards the West. Such auto cyclic behavior is commonly observed in submarine fans [*Deptuck et al.*, 2008; *Shanmugam and Moiola*, 1991].

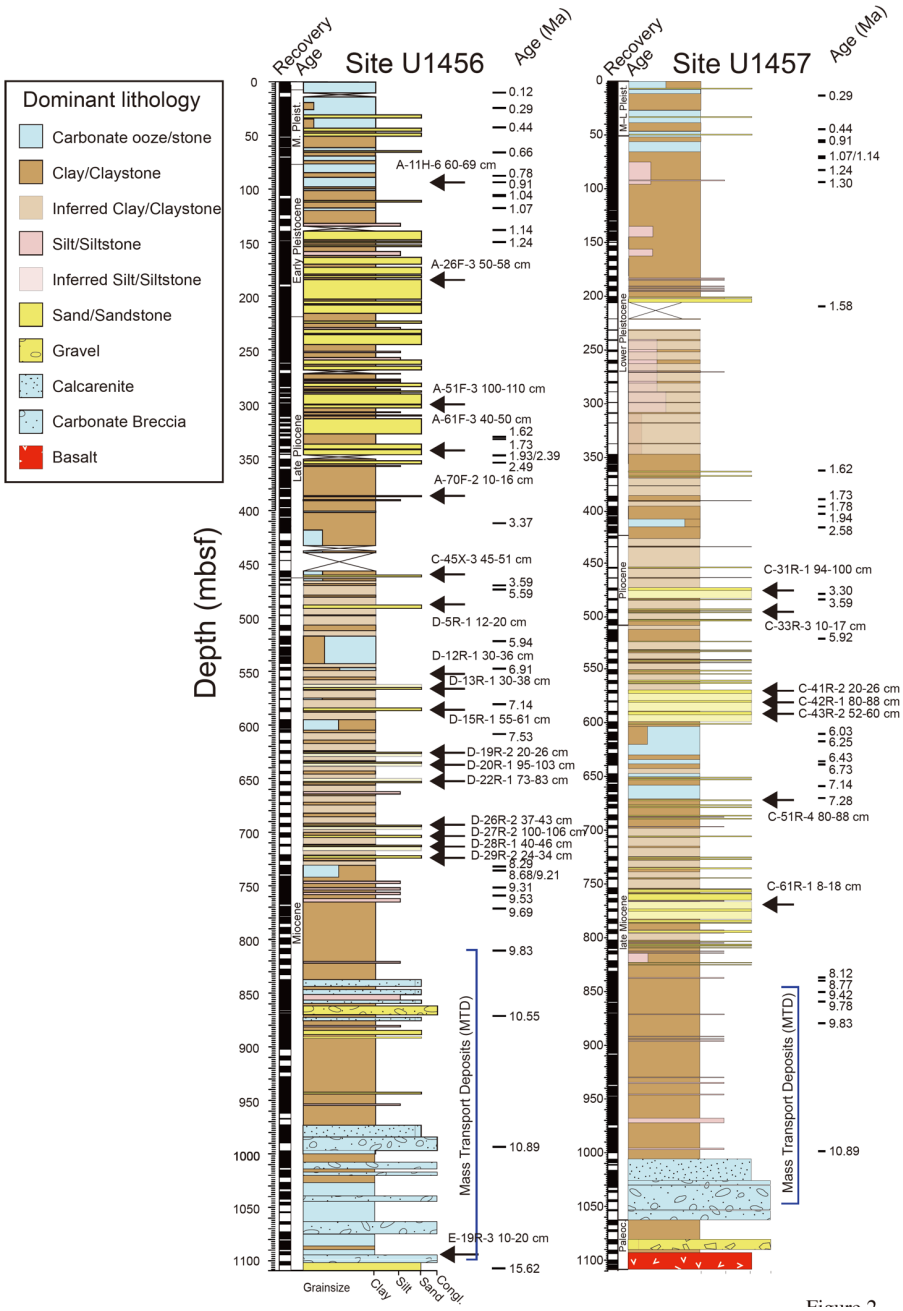

233

234 **Figure 2.** Simplified lithologic logs of the two drill sites considered in this study. Black arrows
235 show the location of the samples analyzed. Modified from Pandey *et al.* [2016c]. Pale shaded
236 intervals show inferred lithologies based on small amounts of recovered core. Because induration
237 is progressive and there is no sharp division, we make no attempt to distinguish between
238 sediments and indurated rocks. Numerical ages are from Pandey *et al.* [2016a] for Site U1456
239 and from Pandey *et al.* [2016b] for Site U1457, with updates from Routledge *et al.* [2019].

240

4 Methods

U-Pb geochronology of detrital zircon grains has become a powerful and widely employed tool for discerning provenance in siliciclastic sedimentary systems. The methodology is based on the concept that different bedrock source rocks are characterized by distinct and/or different age populations of zircons. A zircon budget is not the same as an eroded rock budget because of differences in the relative fertility of bedrock sources with regard to zircon. Zr concentrations have been used as a proxy for the relative abundance of zircons in sediment [*Amidon et al.*, 2005], but the reliability of this approach has recently been questioned [*Malusà et al.*, 2016]. Malusà *et al.* [2016] developed a method using mineralogy and density data from the sediment to infer the fertility of the source bedrock. Unfortunately, this approach is not practical for this work because the sample sizes available from IODP were small (<50 cm^3) so that all the material had to be processed for zircon extraction and even required amalgamating neighboring samples in order to generate enough data to make a statistically meaningful result in some cases. We use previously published geochemical data from modern rivers as a guide to zircon fertility as this data already exists and we cross check this prediction against other provenance methods to assess its credibility. Our erosion budgets are however largely zircon based, not bulk sediment.

Zircon is a robust mineral and its grains do not generally experience significant physical abrasion during transport, unless they had previously accumulated major radiation damage. Hence, zircon can undergo multiple episodes of recycling and redeposition. Although the concentration of zircon in any given sediment can be affected by hydrodynamic sorting, this process may not be a strong influence on the resulting detrital age spectra unless there is a relationship between grain size and crystallization age, which we investigate below. Work on Yangtze River sediments indicates that the typical grain size range analyzed using LA-ICP-MS technology is representative of the overall population in the sediment without a bias related to grains size [*Yang et al.*, 2012]. Detrital zircon U-Pb dating has been widely applied in provenance studies in the Western Himalaya due to the large range of zircon U-Pb age differences between the various source terrains described above. Furthermore, studies of the modern Indus River documented a close correlation between the modern zircon U-Pb age spectra and the bedrock sources, albeit one implying focused erosion in several sub-basins [*Alizai et al.*, 2011; *Zhuang et al.*, 2018]. Several studies have also used detrital zircon dating to investigate the provenance of the Siwalik Group foreland basin sedimentary rocks [*Baral et al.*, 2015; *Bernet et al.*, 2006; *DeCelles et al.*, 2004; *Zhuang et al.*, 2015] and Quaternary sediments in the delta and offshore [*Clift et al.*, 2008a; *Li et al.*, 2019], allowing evolving erosion patterns to be reconstructed.

4.1 Major Element Analyses

In addition to detrital zircon U-Pb dating, bulk sediment samples were analyzed for their major element contents by Inductively Coupled Plasma Emission Spectrometry (ICP-ES) at Boston University (BU), USA. Sediment samples were decarbonated with acetic acid, washed with distilled and deionized water with a purity of 9–12 megaohms, and hand powdered at Louisiana State University (LSU) before total fusion preparation at BU. Glass beads for each sample were made in a muffle furnace under 1050˚C by fusing 100 ± 0.5 mg of sample mixed

with 400 ± 0.5 mg lithium metaborate ($LiBO_2$). The melted mixture was then dissolved in 5% HNO_3, sonicated, manually shaken until no visible grains were observed, and further diluted for analysis [*Dunlea et al.*, 2015]. Precision for all elements was better than 1% of the measured value, and accuracy was confirmed by repeated analyses of International Standard Reference Materials (Basalt, Hawaiian Volcano Observatory, BHVO-2)[*Wilson*, 1997]. Results of the geochemical measurements are shown in Table 1.

4.2 Grain size Analysis

For quantitative grain size analysis, samples were prepared using standard procedures as described by Howell *et al.* [2014]. We put a small amount of sample into a cleaned 50 ml plastic centrifuge tube and added 5–7 ml of sodium phosphate solution. The tube was capped and vortexed to deflocculate clay-sized sediment and separate organic particles. The sample was poured through an 850 µm sieve and funneled into a 15 ml glass test tube. After centrifuging and removing the clear supernatant, 2–3 ml of sodium phosphate and 5 ml of 30% H2O2 were added. Tubes were vortexed again and then put into a hot bath that was heated to 70˚C. This step requires persistent monitoring to prevent loss of reactant by spraying it with acetone until the reaction is stabilized. Reactants then sat overnight to completely oxidize organic matter. Reacted supernatant was removed, and 5 ml of sodium phosphate was added. These treated samples were then rinsed with deionized water, transferred into clean 50 ml plastic centrifuge tubes, and topped with sodium phosphate into a sample solution of up to 40 ml. Samples were vortexed again prior to grain size analysis. Grain size analysis was conducted on a Beckmann Coulter LS13 320 laser diffraction particle size analyzer at LSU. The obscuration of all running samples in the aqueous liquid module (ALM) was between 8–12 %. Result of the analysis are provided in Table 2.

4.3 Zircon U-Pb dating

After standard mineral separation, zircon grains were sprinkle-mounted onto double-sided tape on 1” acrylic discs and analyzed at random using depth-profiling LA-ICP-MS U-Pb geochronology [*Marsh and Stockli*, 2015]. Although this method differs from the more common analysis of cut and polished grains there is no indication that this profiling approach yields results that differ significantly from earlier work, including work done in the Himalaya [*Colleps et al.*, 2019]. For each sample at least 120 zircons were analyzed to obtain provenance datasets that resolve all components that comprise >5% of the total population [*Vermeesch*, 2004]. The analyses were completed using a PhotonMachine Analyte G.2 Excimer laser (30 µm laser spot size) with a large-volume Helex sample cell and a Thermo Element2 ICP-MS using procedures described in Hart *et al.* [2016] at the UTChron facilities at the Jackson School of Geosciences at the University of Texas at Austin. GJ1 was used as the primary reference standard [*Jackson et al.*, 2004] and a secondary in-house zircon standard (Pak1 with a TIMS $^{206}Pb/^{239}U$ age of 43.0 Ma). The data from the analyses were then reduced using the Iolite data reduction software VizualAge [*Paton et al.*, 2011; *Petrus and Kamber*, 2012]. For analyzed detrital zircons, the $^{206}Pb/^{238}U$ age was used for grains younger than 850 Ma and the $^{207}Pb/^{206}Pb$ age was used for grains older than 850 Ma [*Gehrels et al.*, 2008]. All ages reported use 2σ absolute propagated uncertainties. $^{207}Pb/^{206}Pb$ ages are less than 30% discordant, and $^{206}Pb/^{238}U$ ages are less than 10% discordant [*Gehrels et al.*, 2011]. The discordance reported is calculated with the $^{206}Pb/^{238}U$

and $^{207}Pb/^{235}U$ ages if <850 Ma and the $^{206}Pb/^{238}U$ and $^{207}Pb/^{206}Pb$ ages if >850 Ma. Although some studies have suggested older crossovers between the $^{206}Pb/^{238}U$ and $^{207}Pb/^{235}U$ ages and the $^{206}Pb/^{238}U$ and $^{207}Pb/^{206}Pb$ ages (e.g., 1.5 Ga [*Spencer et al.*, 2016]) blindly picking a crossover at 1.5 Ga leads to culling of discordant $^{206}Pb/^{238}U$ ages, or unacceptable smearing and loss of age mode definition between 800–1500 Ma for many samples. Picking a 1500 Ma crossover cutoff and a 20% discordance filter would result in the loss of 80% of the data between 850 and 1500 Ma making the data bad provenance proxies. The 850 Ma crossover was chosen in accordance with the approach of Spencer et al. [2016] and Marsh et al. [2019]. The data are reported in Table 3.

When accurately dating a geological event, high concordance is a requirement but when assigning grains to broad age populations for provenance work the emphasis is on high numbers of grains rather than on high precision in order to improve the statistical reliability. The appropriate level of discordance filter needs to be determined for each data set in light of the goals of the study and the complexities encountered. If a study yields a mix of Phanerozoic and Archean ages, and the relative proportions of these ages are important, a generous (e.g., 30%) discordance cutoff is appropriate so that most Precambrian ages are retained [*Gehrels*, 2012].

5 Results

5.1 Grain-size of sediments

The sediments were assessed using the classification scheme of Folk [1974](Fig. 3). Sediments range from silty sand to silt and mud, both the new samples processed here and those from the earlier study we integrate with here {Clift, 2019 #152}. The grain size variation in single samples can be better assessed by plotting the proportion of each grain size fraction as a spectrum (Fig. 4). We see generally good sorting (positive kurtosis) and a negative skew, meaning a dominance of the finer grain sizes and a tail of coarser grains comprising a diminishing proportion of the sediment. This is especially true for the coarsest grained sediments. The vast majority of the sediment considered here is classified as fine sand to silt, with only small amounts of medium and coarse sand in a minority of samples, three from Site U1456 dated at 1.92–1.32 Ma and one from Site U1457 at 3.02 Ma. Three of the new samples do contain significant volumes of medium and even coarse sand (3.39, 7.00 and 7.27 Ma). The spot size of the laser used for the U-Pb dating means that grains smaller than ~30 μm were not considered in this study. Depending on the sample this represents a wide range of the total sediment load. Only 9% of Sample U1456A-51F-3, 100-110 cm was less than 30 μm, while 89% of Sample U1456A-70F-2, 10-16 cm is smaller than that threshold. See Table 2 for full results.

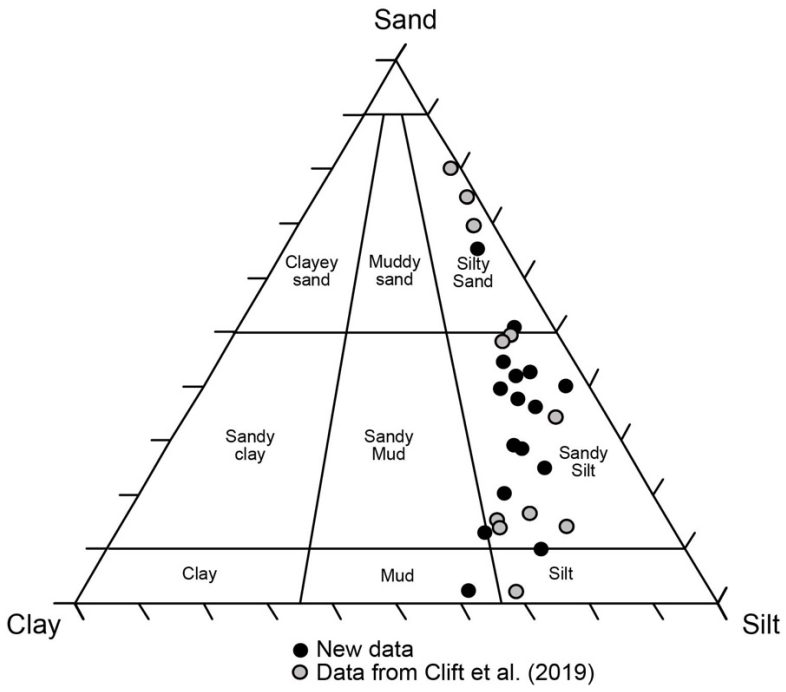

Figure 3. Grainsize range of all samples analyzed for U-Pb zircon dating from the Laxmi Basin shown on the scheme of Folk [1974]. Samples are marked to show those published by Clift *et al.* [2019b], rather than presented new here (Table 2). Note the dominance of silty sand and sandy silt in the analyzed samples.

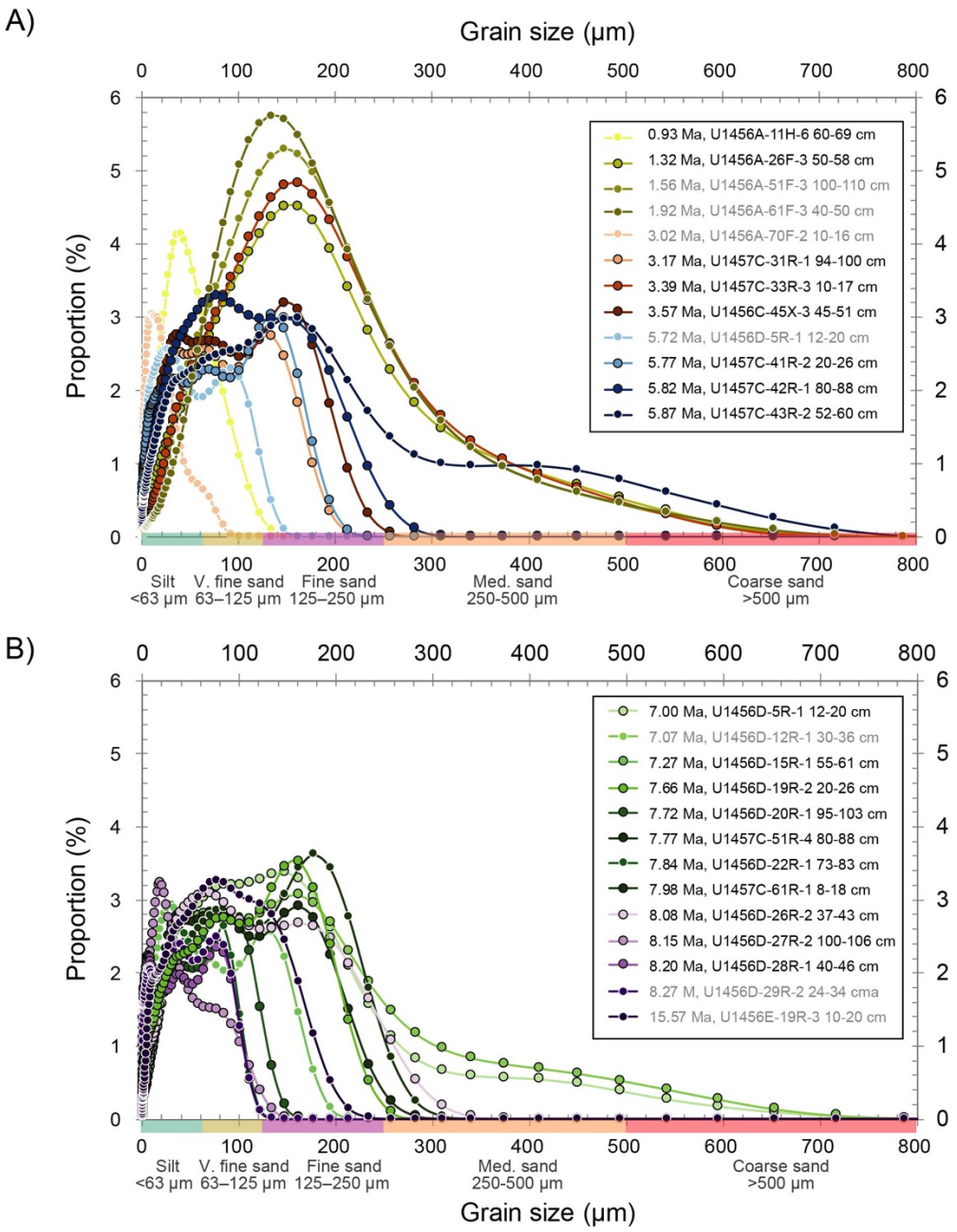

Figure 4. Detailed grain size spectra showing the range of sizes of the different samples considered within this study. Most of the sediment is fine sand to coarse silt in size and typically shows a coarse-skewed. A) Samples younger than 7 Ma, b) samples older than 7 Ma. Samples are marked to show those published by Clift *et al.* [2019b](gray text labels and white ringed symbol), rather than presented new here (Table 2) (black text labels and black ringed symbol).

5.2 Bulk Sediment Chemistry

The general geochemical character of the sediments can be seen on a CN-A-K ternary diagram [*Fedo et al.*, 1995](Fig. 5A). The IODP samples plot in an array with a Chemical Index of Alteration (CIA) of ~65 to 73 [*Nesbitt et al.*, 1980]. They form a roughly linear array trending towards the illite end member and suggestive of its progressive involvement as the primary mineral breakdown product. The Laxmi Basin samples can be compared with sediments from the Quaternary Indus delta [*Clift et al.*, 2010], Indus Canyon [*Li et al.*, 2018], the Indus Marine A-1 borehole, as well as modern sediments from the western Indian shelf and slope between the Saurashtra peninsula and Bhatikal [*Kurian et al.*, 2013](Fig. 1). Rivers south of Bhatikal have a different composition and are unlikely to be sources to the Laxmi Basin sites.

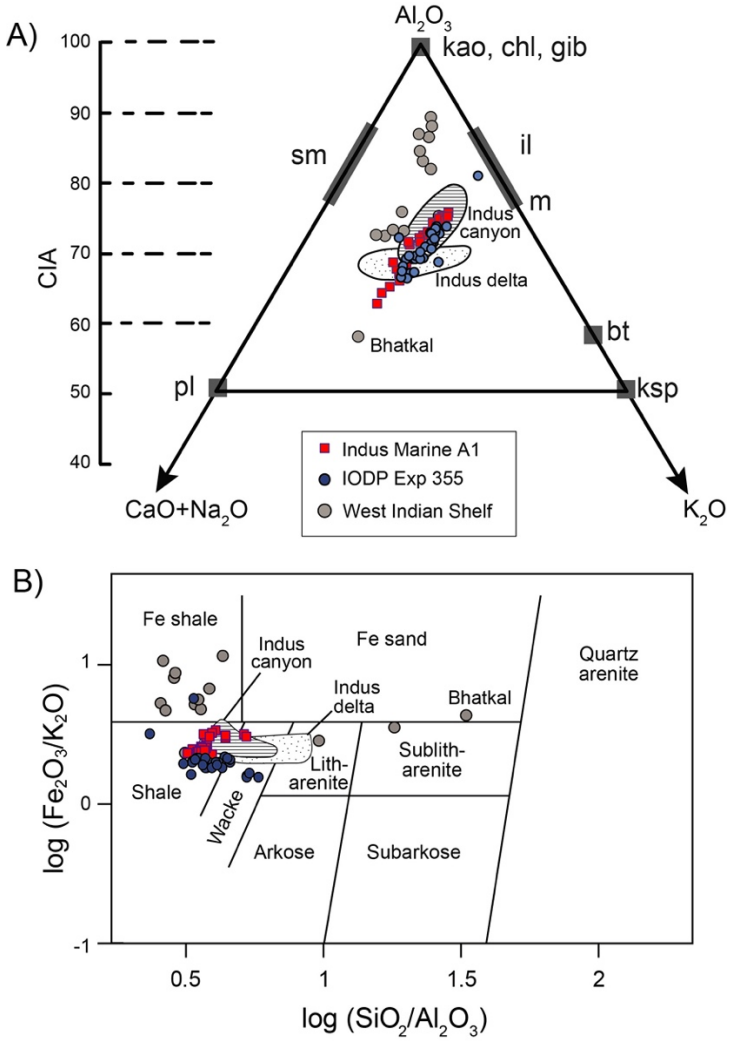

Figure 5. (A) Geochemical signature of the analyzed samples illustrated by a CN-A-K ternary diagram [Fedo *et al.*, 1995]. CN denotes the mole weight of Na_2O and CaO* (CaO* represent the CaO associated with silicate, excluding all the carbonate). A and K indicate the content of Al_2O_3 and K_2O respectively. Samples closer to A are rich in kaolinite, chlorite and/or gibbsite (representing by kao, chl and gib). CIA values are also calculated and shown on the left side,

with its values are correlated with the CN-A-K. Samples from the delta have the lowest values of CIA and indicates high contents of CaO and Na_2O and plagioclase. Abbreviations: sm (smectite), pl (plagioclase), ksp (K-feldspar), il (illite), m (muscovite). B) Geochemical classification of sediments from this study as well as those from the Indus delta [*Clift et al.*, 2010], Indus Canyon [Li *et al.*, 2018] and western Indian shelf [Kurian *et al.*, 2013] following the scheme of Herron [1988].

The Laxmi Basin sands have very similar bulk compositions to the Quaternary Indus canyon and delta, as well as the Indus Marine A-1 samples (Fig. 5A), but plot below or to the right of the array of the western Indian shelf sediments. Only the shelf sample taken near Bhatikal (the southernmost shelf sample that overlies the Precambrian crystalline basement of India, rather than the Deccan Traps), plots below the Laxmi Basin sediments, with a lower CIA value. This plot confirms that the analyzed sands have little in common with material eroded from peninsular India and appear consistent with an Indus River origin. Likewise, the sediments plot close to the Quaternary Indus sediments and those of Indus Marine A-1 on the discrimination diagram of Herron [1988](Fig. 5B). The IODP samples plot with slightly lower Fe_2O_3/K_2O values compared to the proximal sediments. The Laxmi Basin sediments form an array defined as shales and wackes, while the western Indian shelf sediments fall into the Fe shale, litharenite, sublitharenite and Fe sand fields.

We further assess whether grain size has any relationship to zircon concentrations by plotting Zr contents against median grain size (Fig. 6). Although the original source characteristics and hydrodynamic sorting of the sediment might be expected to concentrate zircons in certain size fractions this does not appear to be a significant factor within the range of grain sizes considered here.

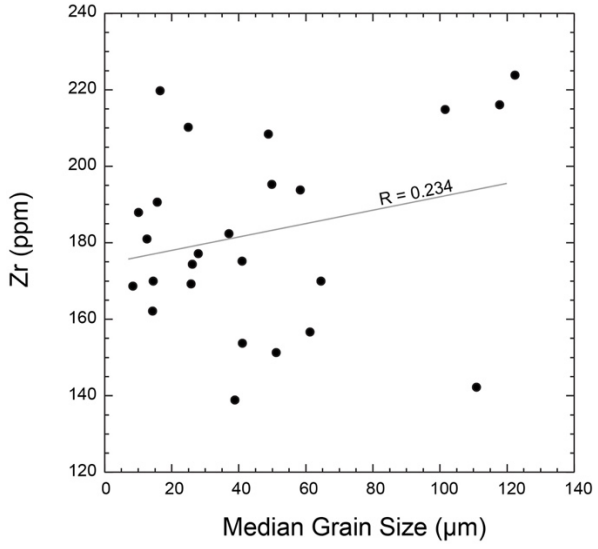

Figure 6. Cross plot of Zr concentration against median sample grain size. No strong correlation is observed.

5.3 Detrital Zircon U-Pb

We examined the range of zircon U-Pb ages using a kernel density estimate (KDE) diagram (Fig. 7) to assess similarities between different sampled sediments and potential source regions (Fig. 7). All of the sediments analyzed in this study show a significant zircon U-Pb component younger than 200 Ma. In addition, we see significant components dated at 350–1250 Ma and 1500–2300 Ma. The abundance of these older age components overall increases with decreasing sample depositional age. The 350–1250 Ma age component appears to increase in all sediment samples dated at 5.87 Ma or younger compared to the older sediments. A particularly prominent age mode at ~1800 Ma first occurs in sediments deposited at 3.43 Ma and becomes extremely prominent in all samples younger than 1.92 Ma. This age mode is also observed in the modern sediment from the Indus river mouth [*Clift et al.*, 2004].

Examining the <200 Ma zircon U-Pb ages in detail, we see that the vast majority of grains are younger than 120 Ma with prominent age peaks at around 100–120 Ma and 40–70 Ma (Fig. 8). In the youngest samples, especially those deposited starting at 3.02 Ma, we see another age mode at ~20 Ma, although this is also seen in the sample dated at 5.78 Ma. One sample deposited at 3.17 Ma differs in its <200 Ma age spectra from the other samples as it is characterized by a prominent age peak at 100–120 Ma, with a general lack of other young zircon grains.

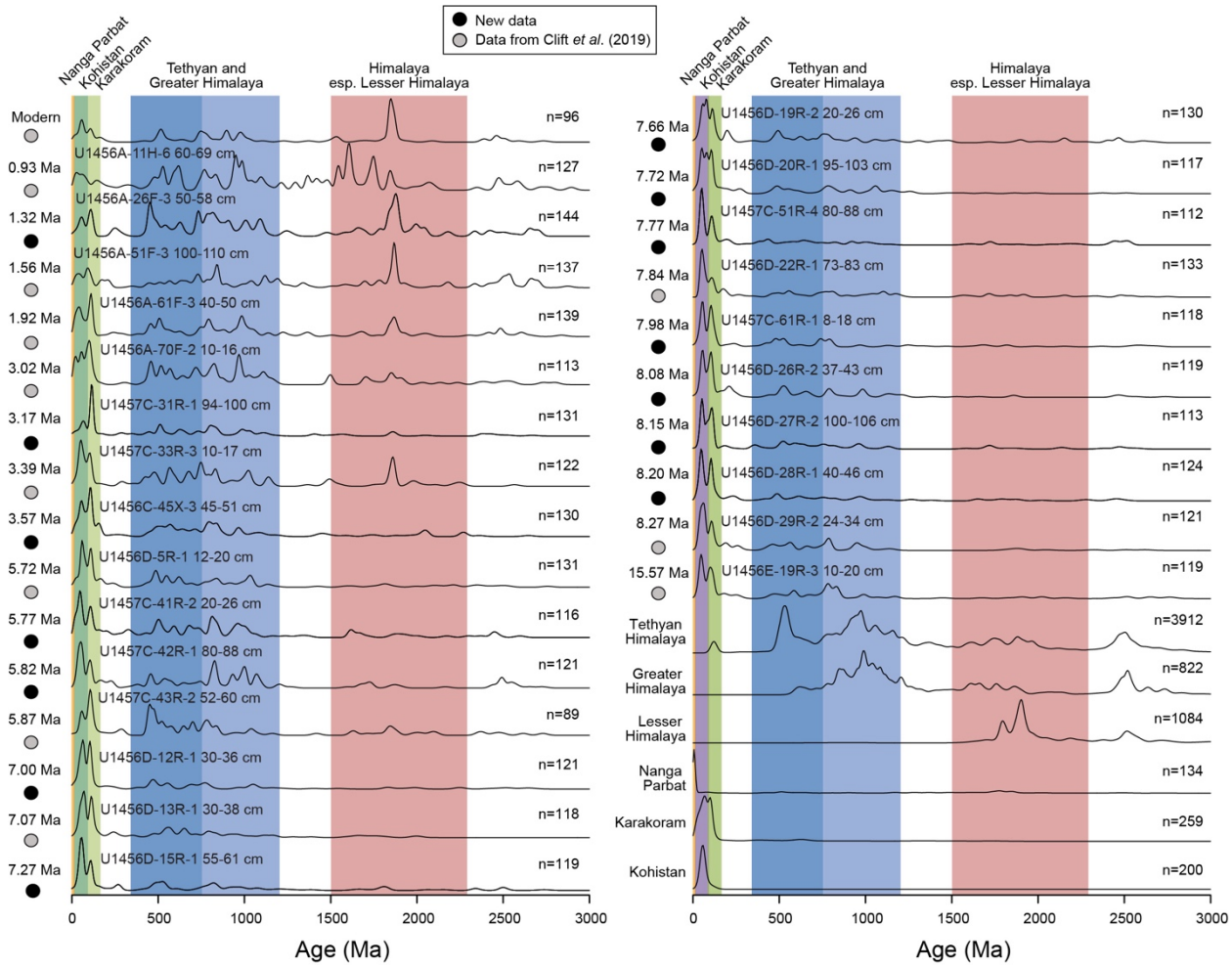

Figure 7. Kernal density estimate (KDE) diagram showing the range of the zircon U-Pb ages for individual sand grains back to 3000 Ma. Colored strips show the range of populations with diagnostic links to critical source terrains in the headwaters of the Indus. Data from the Siwaliks, as well as the Tethyan, Greater and Lesser Himalaya are compiled from DeCelles *et al.* [2004]. Karakoram data is from is from Le Fort *et al.* [1983], Parrish and Tirrul [1989], Schärer *et al.* [1990], Fraser *et al.* [2001] and Ravikant *et al.* [2009]. Nanga Parbat data is from Zeitler and Chamberlain [1991] and Zeitler *et al.* [1993]. Transhimalayan data is from Honegger *et al.* [1982], Schärer *et al.* [1984], Krol *et al.* [1996], Weinberg and Dunlap [2000], Zeilinger *et al.* [2001], Dunlap and Wysoczanski [2002], Singh *et al.* [2007], and Ravikant *et al.* [2009]. Samples are marked to show those published by Clift *et al.* [2019b], and those presented new here.

6 Discussion

Major element discrimination diagrams (Fig. 5) suggest that the Laxmi Basin sediments are most similar to deposits found in the Quaternary and modern Indus River/delta/canyon, as well as the older sedimentary rocks from Indus Marine A-1 (Fig. 5). However, they are distinctly

449 different from sediments sampled from the modern western Indian shelf, and largely derived
450 from the Deccan Plateau and underlying units [*Kurian et al.*, 2013]. These geochemical data
451 suggest that the Laxmi Basin sediments, most likely originated from the Indus River mouth.

452 We assessed the overall geochemical characteristics of the sediments by plotting the
453 major element composition of each sample normalized to the upper continental crust (UCC; Fig.
454 9)[*Taylor and McLennan*, 1995]. Most of the samples display a relatively uniform topology in
455 these diagrams and are broadly similar to both post-LGM sediments from the Indus Delta (KB-
456 40-4), the Holocene delta (TH-10-1) and, the modern Indus river (Thatta TH-1). Most of the
457 samples show a similar major element composition compared to the UCC, with a consistent
458 enrichment in TiO_2, suggestive of a higher content of Ti-bearing heavy minerals (e.g., rutile,
459 anatase, brookite, ilmenite, titanite). This enrichment is particularly strong in the 0.93 Ma sample
460 which apatite fission track data indicate to have a unique provenance [*Zhou et al.*, 2019]. There
461 are also relative depletions in CaO and Na_2O, as well as P_2O_5, implying both a lower plagioclase
462 and apatite content relative to the UCC. This relative depletion in CaO is strongest in the modern
463 river mouth sediment and weakest in the post-glacial delta sediments, with the fan sediments
464 plotting between these extremes. The systematically lower abundance of plagioclase and apatite
465 likely reflects chemical weathering in the floodplains prior to deposition in the ocean, because
466 these phases are less stable under conditions dominated by chemical weathering [*Guidry and*
467 *Mackenzie*, 2000; *White and Brantley*, 1995]. However, all samples show this effect and there is
468 a general consistency in the overall composition, we conclude that we are comparing sediments
469 of a similar bulk character. All fan sediments show Zr abundances relatively close to the UCC
470 average.

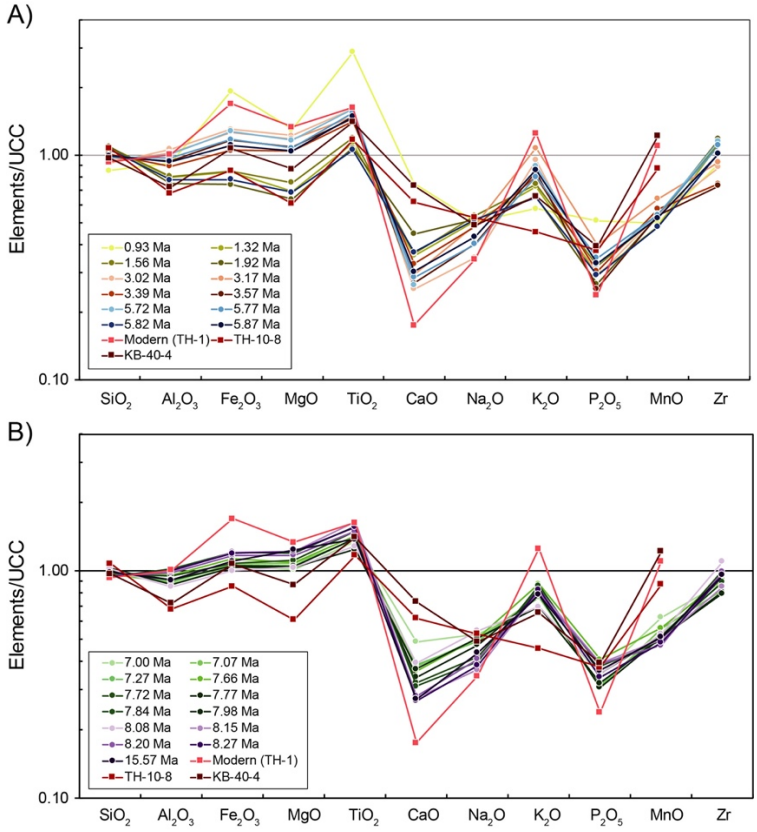

471

Figure 9. Upper continental crust normalized compositions of the sediments whose zircons are the focus of the study. Bulk settlement compositions are normalized according to the average of the continental crust from Taylor and McLennan [1995].

6.1 Changing Provenance

Before using the changing zircon U-Pb age spectra to infer changing sediment provenance we examine the possible role of grain size in controlling the results. Sediment grains are fractionated during transport because different densities and shapes affect their settling characteristics [*Garzanti et al.*, 2009]. Zircons all have the same density but the size and shape of the grains from a given source may vary and influence the final conclusions. If one source is associated with smaller or larger grains compared to other sources then this may prejudice the analysis, especially if the grains are too small to be analyzed. Garzanti *et al.* [2009] concluded that this effect was moderate in the Ganges-Brahmaputra catchment, which has strong similarities to the Indus. We plot major, provenance-related age populations (0–25, 40–70, 70–120, 300–750, 750–1250 and 1500–2300 Ma) against median grain size for all samples considered here to see if grain size plays a strong role in controlling the age spectra. Figure 10 shows that there is not a strong correlation between sediment median grain size and the proportion of various provenance-sensitive age groups. However, we note that the four coarsest sediments (>100 μm) do contain more 750–1250 and 1500–2300 Ma grains compared to the 40–70 and 70–120 Ma groups. The effect is especially strong with the 1500–2300 Ma group. In contrast to work on the Amazon River by Lawrence *et al.* [2011] who showed that older grains were significantly smaller than younger ones, the reverse may be true in the Indus. It is however noteworthy that the coarser sediments are all young 3.02 Ma and younger and as demonstrated below the provenance inferred from similar aged finer sediment is not greatly different and also consistent with neighboring bulk sediment Nd isotope constraints. We conclude that there may be a grain size issue with the coarsest sediment, but that this is not dominant in controlling the U-Pb age spectra.

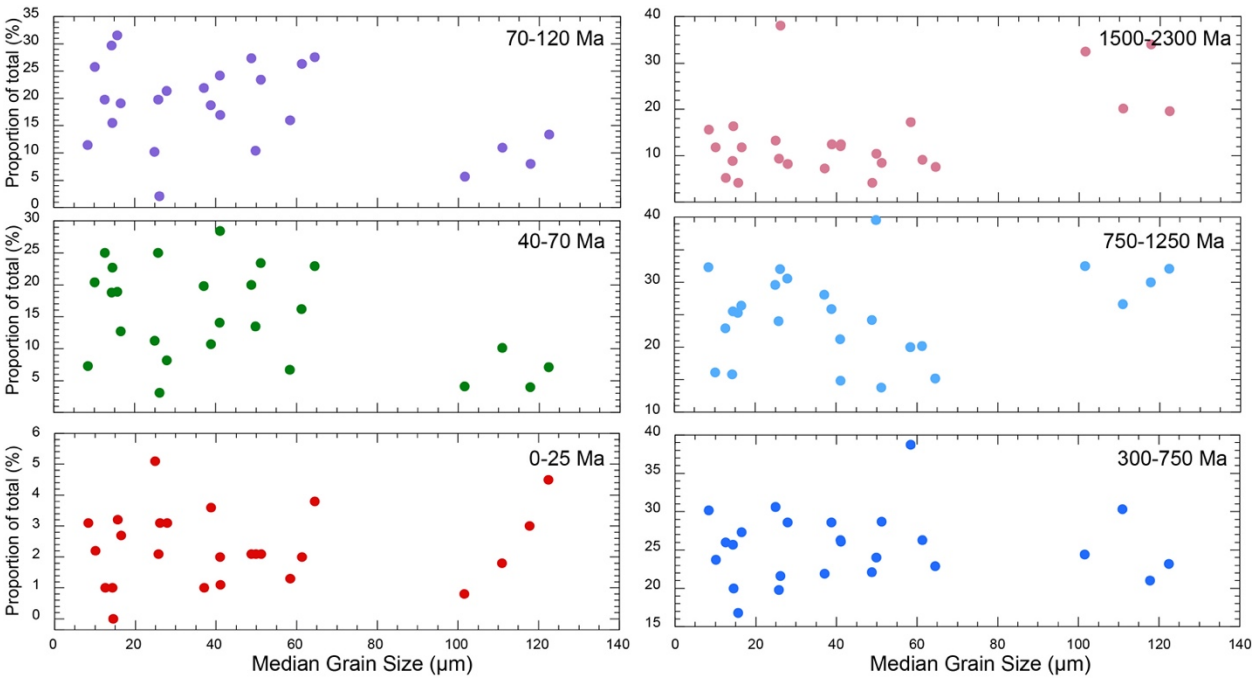

Figure 10. Plots of relative abundance of provenance sensitive zircon age populations in individual samples compared with sample median grain size. The coarsest samples show preference for the oldest U-Pb ages and a relative lack of the younger populations.

The zircon U-Pb age spectra are used to track the source evolution of sediment reaching the Arabian Sea and compared to bedrock zircon U-Pb age signatures of possible source areas (Fig. 7). The abundance of grains younger than 200 Ma correlates well with young bedrock from the Indus Suture Zone, particularly in Kohistan, the Transhimalaya and Karakoram, as well as Nanga Parbat (Fig. 8). The abundance of these young zircon grains clearly points to sediment being supplied by the Indus River and not by peninsular India, where no magmatism <200 Ma is known outside the Deccan Plateau. Detrital zircon grains older than 350 Ma also largely correlate with various bedrock sources known in the Himalaya. Detrital zircon age modes between 350 and 750 Ma have been correlated with bedrock sources in the Tethyan Himalaya [*Alizai et al.*, 2011], although it is generally agreed that there is little real difference in terms of U-Pb ages, between Tethyan and Greater Himalaya zircon signatures [*Gehrels et al.*, 2011], and these are in any case not always mapped consistently by different groups [*Webb*, 2013]. Consequently, zircons with ages between 350 and 1250 Ma could be derived from either source. The older samples show relatively low abundance of grains in this age range, but these increased significantly starting at 5.87 Ma and become very abundant in the last few million years. Older grains, dating between 1500 and 2300 Ma, are particularly common in Lesser Himalayan sources, although they are also present in smaller amounts in the Tethyan and Greater Himalaya [*DeCelles et al.*, 2000; *Gehrels et al.*, 2011]. These mainly Paleoproterozoic zircon grains are almost entirely absent from the Laxmi Basin Miocene samples, but show a marked increase beginning at 5.72 Ma, and becoming very abundant beginning at 1.56 Ma (Fig. 7). We therefore interpret these patterns to indicate a progressive increase in erosion from the Himalaya starting

after 7.0 Ma, and especially starting at 5.72 Ma, with strong erosion from the Tethyan and Greater Himalaya. After 3.02 Ma there is a dramatic increase in erosional flux from the Lesser Himalaya, which have had a strong influence on the river system since the onset of the Holocene [*Clift et al.*, 2004; *Clift et al.*, 2008a].

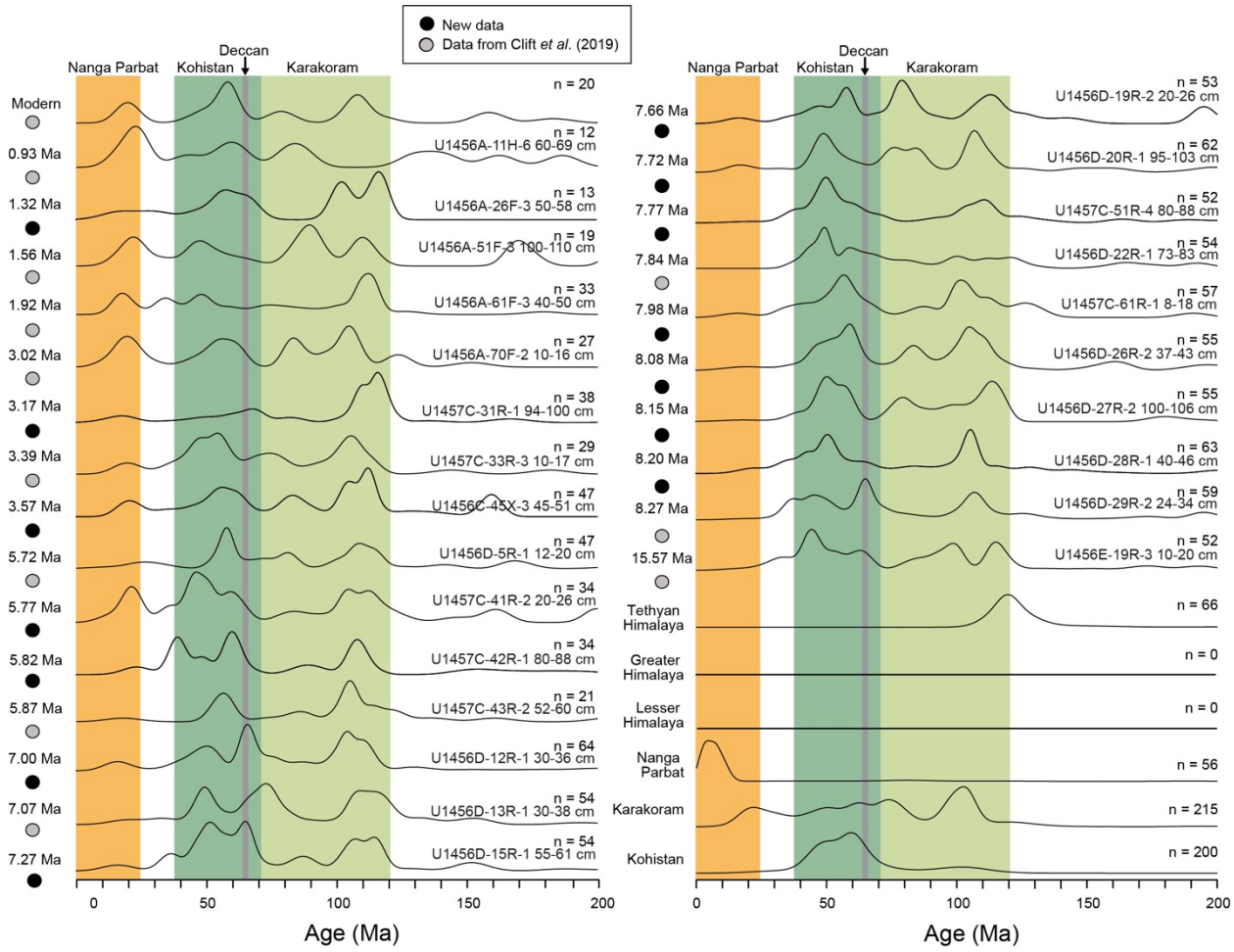

Figure 8. Kernal density estimate (KDE) diagram showing the range of the zircon U-Pb ages for individual sand grains back to 200 Ma. Colored strips show the range of populations with diagnostic links to critical source terrains in the headwaters. See Figure 6 caption for data sources.

If we only consider the zircon grains younger than 200 Ma then we can see that there is evidence of erosion, from both Kohistan and from the Karakoram, in most of the samples analyzed (Fig. 8). Kohistan is particularly noteworthy for having zircon dated between 40 and 70 Ma [*Alizai et al.*, 2011; *Zhuang et al.*, 2018], although there are similar aged units in the Karakoram as well. However, zircon grains older than 70 Ma but younger than 120 Ma are almost exclusively known only from Karakoram bedrock sources [*Searle*, 1996]. The 3.17 Ma

sample does not show the younger 40–70 Ma population, suggesting that it did not receive any significant material from Kohistan/Ladakh.

The youngest (<25 Ma) zircon grains are more enigmatic in terms of their provenance. While very young zircons are known from the present-day Nanga Parbat massif, these are generally younger even than the 25 Ma zircon U-Pb age component observed in many of the samples [*Zeitler et al.*, 1993]. Our new data also show an increased influx from bedrock sources with very young zircon starting at 3.02 Ma, as well as a brief appearance at around 5.78 Ma. It is possible that this increase starting at 3.02 Ma reflects the emergence of Nanga Parbat, although we cannot exclude the influence of other young sources in the southern Karakoram metamorphic belt, which also contains rocks of this age and have experienced very rapid exhumation in the last few million years [*Wallis et al.*, 2016]. Because the Deccan Plateau volcanic rocks were erupted rather quickly around 65 Ma, it is hard to completely exclude their influence because grains of a similar age are also known in Kohistan, and in the Karakoram. However, the erosion from the Deccan Plateau would not account for the other young grains and an influx from that area should result in a clear peak age at 65 Ma, which is not observed.

We also assessed the evolving provenance patterns of sediments in Laxmi Basin using a multidimensional scalar (MDS) analysis of the detrital zircon U-Pb dates [*Vermeesch et al.*, 2016]. In this plot, which is a type of principle component analysis, samples with similar age spectra plot close to one another, while distinct samples are far separated. Figure 11A shows all the detrital samples data, along with a modern river mouth and a delta sample (KB-40) dating from shortly after the LGM [*Clift et al.*, 2008a]. The MDS analysis shows clear and coherent patterns. Samples deposited at and after 1.56 Ma, are relatively similar to the modern river. In contrast, the oldest samples plot in a cluster suggesting a similar Miocene provenance and a subsequent progressive shift from right to left with decreasing depositional age, although with some reversals, most notably at 3.17 and 3.57 Ma. This reflects an overall shift in the zircon age spectra through time. Nonetheless, the LGM sample has stronger similarities with sediments deposited on the fan during the Late Miocene. Earlier work implied that erosion during the LGM was focused in the Karakoram [*Clift et al.*, 2008a] compared to the modern river or during the Holocene when the summer monsoon was strong [*Caley et al.*, 2014; *Fleitmann et al.*, 2003; *Gupta et al.*, 2003]. The new data indicate that older Miocene samples were also deriving their material from Karakoram sources, and this was followed by a shift to more Himalayan sources, especially in the last few million years. The plot implies that the change might be step wise, with a change starting between 7.0 and 5.87 Ma and again at 1.56 Ma.

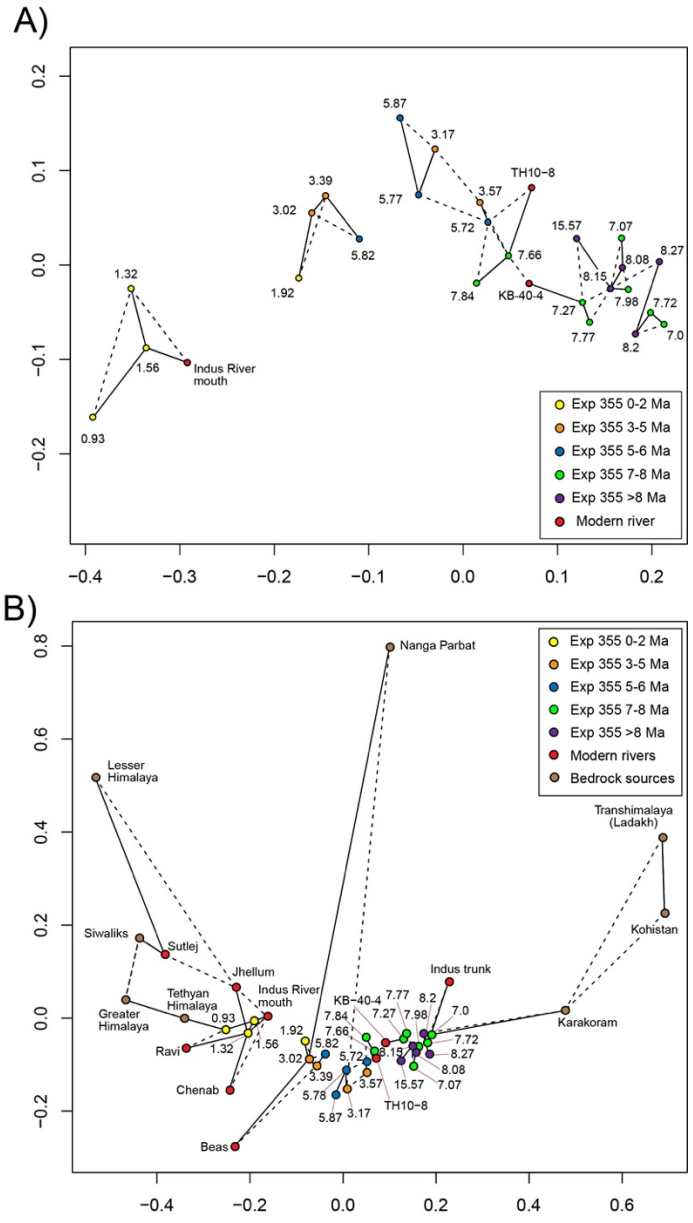

Figure 11. Multidimensional scalar (MDS) diagrams made from zircon U-Pb age data showing (A) how the different sediment samples from IODP Expedition 355 compare with one another and post-glacial sediments from the Indus delta (TH-10-8 and KB-40-4) and (B) with the major source terranes in the Indus catchment, as well as the modern rivers of the Indus catchment, i.e., the main or trunk stream of the Indus, upstream of Attock, and its major eastern tributaries. Solid lines join sediments to their most similar neighbor, while dashed lines join the next most similar. Sources of bedrock age data come from the literature, as described in Figure 6. River data is from Alizai *et al.* [2011]. Note that sediments older than 5 Ma plot towards the right in Figure 10B, in the direction of Karakoram bedrock sources, whereas there is a progressive migration towards the left, towards Himalayan sources after that time. Diagram was constructed using the statistical package of Vermeesch *et al.* [2016].

The fact that the youngest turbidite sands are most similar to the modern interglacial river, and not the compositions of the Indus shortly after the LGM, also implies that most of the sediment deposited in the Indus Fan has been eroded during interglacial times when the monsoon was strong, even if final deposition did not occur until the sea level fell during the onset of the subsequent glaciation. We envisage fast interglacial erosion generating great volumes of sediment, which is then mobilized, transported, and delivered to the delta as the rains strengthened [*Jonell et al.*, 2017]. The sediment would then be stored on the shelf or in the upper canyon during sea level high stands before being eroded and redeposited as sea level fell [*Li et al.*, 2018]. This emphasizes the importance of monsoon intensity in controlling erosion and sediment delivery in the Western Himalaya.

We also compared the Arabian Sea sediments with known zircon ages from bedrock sources themselves. Figure 11B shows the progressive changes from the Miocene to the present and emphasizes the fact that the stratigraphically oldest detrital zircon samples plot closest to sources in the Karakoram and have similarities with analyses from the trunk stream (upper reaches) of the main Indus River, before it mixes with the Himalaya-draining Eastern tributaries, such as the Jhellum, Chenab, Ravi, Sutlej and Beas (Fig. 1). Conversely, the stratigraphically youngest sediments plot on this diagram closest to Himalayan sources and have greater similarity not only to the modern river mouth, but also Himalayan tributaries such as the Ravi, Chenab and Jhellum rivers.

These data also imply that Nanga Parbat has not been a very important contributor to the bulk sediment flux. Whether this is actually true or not is not entirely apparent because the bedrock analyses from Nanga Parbat were focused on igneous rocks in the center of that metamorphic massif, and might not be representative of the net erosional flux from this particular source. However, the relationships displayed in Figure 11B can be readily explained as a simple mixing between Karakoram and Himalayan sources, with a progressive shift towards the Himalaya through time.

6.2 Unmixing Sources

In order to further characterize the evolving source of sediments to the Indus Fan we employ the unmixing software of Sundell and Saylor [2017], which analyzes the U-Pb age spectra from each of the samples and compares them with the defined end-member compositions of the different source ranges compiled from the published literature. This approach works particularly well in the western Himalaya where the sources are well defined and often unique. Data from the Tethyan, Greater and Lesser Himalaya were compiled from DeCelles *et al.* [2004]. Data from the Karakoram are from Le Fort *et al.* [1983], Parrish and Tirrul [1989], Schärer *et al.* [1990], Fraser *et al.* [2001] and Ravikant *et al.* [2009]. Data from Nanga Parbat are from Zeitler and Chamberlain [1991] and Zeitler *et al.* [1993]. Data from the Transhimalayan are from Honegger *et al.* [1982], Schärer *et al.* [1984], Krol *et al.* [1996], Weinberg and Dunlap [2000], Zeilinger *et al.* [2001], Dunlap and Wysoczanski [2002], Singh *et al.* [2007], and Ravikant *et al.* [2009].

This unmixing method uses a Monte Carlo approach to estimate the contributions from the different sources that would be required to generate the modes and modal abundances of U-Pb ages seen in the sediment samples. Because this is relatively objective the method is considered robust for analyzing potential source contributions, assuming that the sources themselves have been well characterized. The bedrock sources of the Indus catchment have significant differences between many of them and are some of the best characterized worldwide. Results of the Monte Carlo simulation are provided in Table 4, showing the output using all three statistical comparison methods, cross-correlation, the best V value in the Kuiper test. as well as the best D value in the K-S test. The method involves creating 10,000 model mixed sediments using the defined bedrock source end members. The DZMix software then compares the model with the measured spectra and retains the best 1% of these models in order to estimate which sources were contributing the sampled material. We favor the unmixing models derived from the cross-correlation approach as being geological reasonable and favored by Sundell and Saylor [2017].

The results of our unmixing calculations show a progressive provenance evolution that is consistent with that seen in the MDS diagram (Figs. 11 and 12). The very oldest sample deposited at 15.5 Ma shows a dominance of sediment eroded from the Karakoram and from the Tethyan and Greater Himalaya. Most of the Miocene samples dated between 8.2 and 7.0 Ma are more dominated by material from the Karakoram but also usually show significant Tethyan and Greater Himalayan contributions. This Himalayan component is particularly noteworthy at 7.99, 7.84, 7.78, 7.66, and 7.0 Ma during this interval. The proportion of Karakoram zircons shows a significant decrease starting no later than 5.72 Ma and again at 3.02 Ma. The sediment deposited at 3.17 Ma shows the greatest amount of modeled erosion from Karakoram sources of any sample.

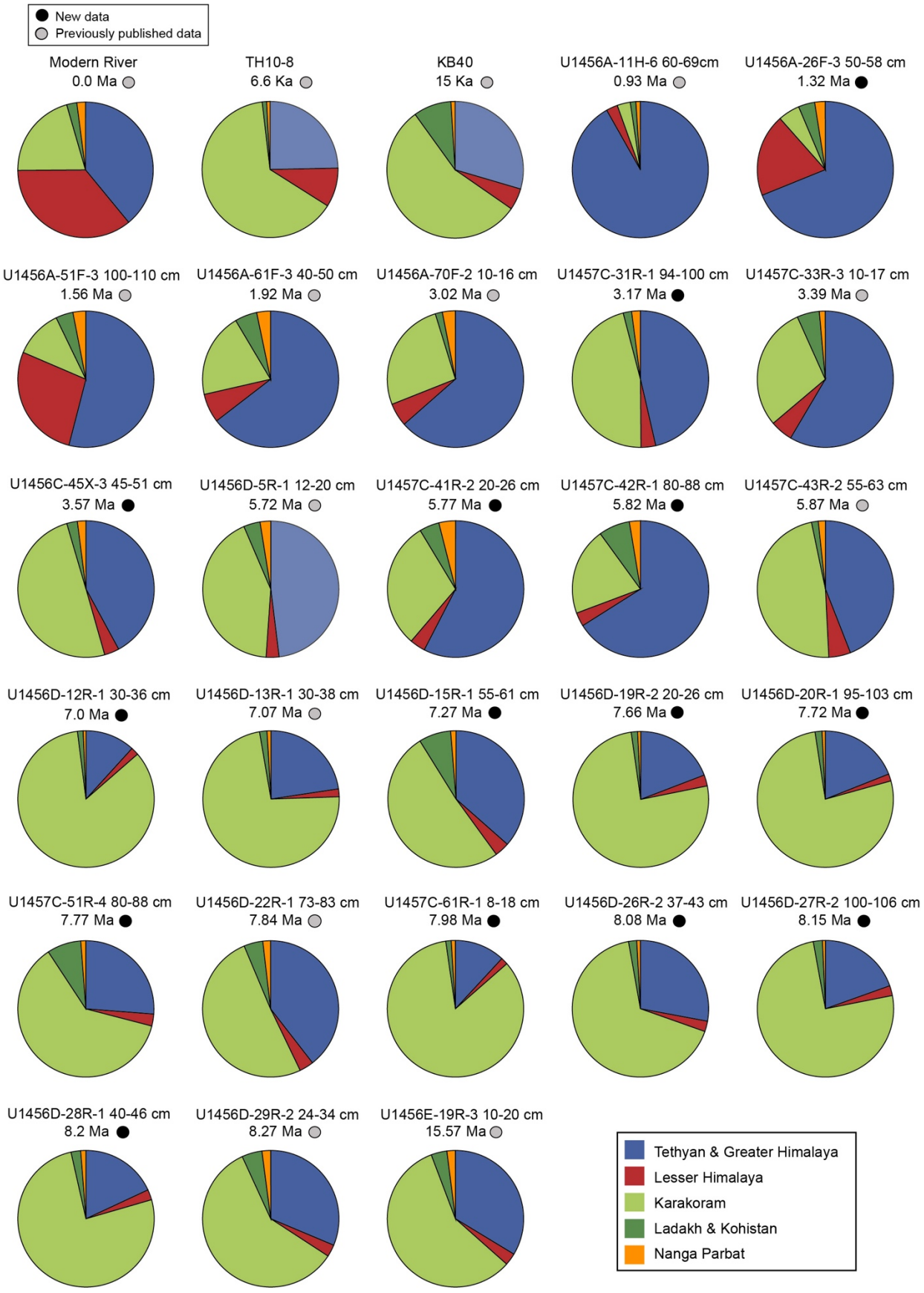
New data
Previously published data
Modern River
0.0 Ma
TH10-8
6.6 Ka
KB40
15 Ka
U1456A-11H-6 60-69cm
0.93 Ma
U1456A-26F-3 50-58 cm
1.32 Ma
U1456A-51F-3 100-110 cm
1.56 Ma
U1456A-61F-3 40-50 cm
1.92 Ma
U1456A-70F-2 10-16 cm
3.02 Ma
U1457C-31R-1 94-100 cm
3.17 Ma
U1457C-33R-3 10-17 cm
3.39 Ma
U1456C-45X-3 45-51 cm
3.57 Ma
U1456D-5R-1 12-20 cm
5.72 Ma
U1457C-41R-2 20-26 cm
5.77 Ma
U1457C-42R-1 80-88 cm
5.82 Ma
U1457C-43R-2 55-63 cm
5.87 Ma
U1456D-12R-1 30-36 cm
7.0 Ma
U1456D-13R-1 30-38 cm
7.07 Ma
U1456D-15R-1 55-61 cm
7.27 Ma
U1456D-19R-2 20-26 cm
7.66 Ma
U1456D-20R-1 95-103 cm
7.72 Ma
U1457C-51R-4 80-88 cm
7.77 Ma
U1456D-22R-1 73-83 cm
7.84 Ma
U1457C-61R-1 8-18 cm
7.98 Ma
U1456D-26R-2 37-43 cm
8.08 Ma
U1456D-27R-2 100-106 cm
8.15 Ma
U1456D-28R-1 40-46 cm
8.2 Ma
U1456D-29R-2 24-34 cm
8.27 Ma
U1456E-19R-3 10-20 cm
15.57 Ma
Tethyan & Greater Himalaya
Lesser Himalaya
Karakoram
Ladakh & Kohistan
Nanga Parbat

650

Figure 12. Pie diagrams showing the predicted source compositions of the zircon populations in sands from the Laxmi Basin as unmixed using the software of Sundell and Saylor [2017]. Note the significant reduction in flux from the Karakoram starting ~5.72 and again at 3.02 Ma. Samples are marked to show those published by Clift *et al.* [2019b], and those presented new here.

From 3.02 Ma onwards the Himalaya dominate as sources to the submarine fan, with significant amounts of material from the Lesser Himalaya first appearing at 1.56 Ma. The sample dated as being deposited at 0.93 Ma is anomalous for being very similar in source signature to Tethyan and Greater Himalayan bed rocks sources. However, we note that fission track data indicate that this sample was derived from peninsular India [*Zhou et al.*, 2019]. The unmixing analysis largely mirrors the pattern shown by the MDS diagram, in showing a progressive long-term increase in erosion from the Himalaya relative to the Karakoram, although with significant steps making the evolution nonlinear. All of the samples contain a small amount of very young <25 Ma zircons. None of the samples analyzed show a close similarity with post-LGM river compositions. Delta samples deposited at 6.6 and 15 ka are strongly enriched in Karakoram-derived grains compared to fan sediments deposited at and after 3.02 Ma. This short term variability is interpreted to reflect the short-term changes in erosion patterns linked to monsoon strength, modulated by glacial cycles since the onset of the NHG.

6.3 Relationships to Climate Change and Tectonics

The progressive increase in the relative flux from the Himalaya since the Middle Miocene represents the progressive unroofing of these units. Structural reconstructions of the Western Himalaya predict that prior to 5.4 Ma the Greater and Lesser Himalaya were not exposed [*Webb*, 2013] implying that the Himalayan contribution was derived entirely from the Tethyan Himalaya during the Miocene. As we are not able to distinguish between Tethyan and Greater Himalaya derived sediment we focused on the first appearance of significant amounts of 1500–2300 Ma, Inner Lesser Himalayan detritus starting at 1.56 Ma. Previous studies considered these ranges to have been exposed somewhat before 1.6 Ma. Study of the Siwalik Group in the area of the Beas River Valley indicated an initial exposure of these units around 9 Ma and significant exposure by 6 Ma based on Nd isotope data [*Najman et al.*, 2009]. Our data support the findings of Clift *et al*. [2019b] that this exposure may only reflect the local situation in the paleo-Beas River area, but that widespread regional exposure of the Inner Lesser Himalayan units comes somewhat later. While Clift *et al*. [2019b]favored increased Inner Lesser Himalaya erosion starting at 1.9 Ma our new zircon data imply that 1.56 Ma is a more accurate age for this this transition.

Our result also contrasts with the suggestion by Myrow *et al.* [2015] that the Inner Lesser Himalaya were widely exposed and eroding by 16 Ma. Although we cannot exclude this from happening further east in the Ganges Basin our data do not support this over a wide area of the western Himalaya until much later.

690 The timing of Lesser Himalayan unroofing may reflect the development of the thrust
691 duplex, which characterizes the structure of the Lesser Himalaya in this area [*Huyghe et al.*,
692 2001; *Webb*, 2013]. Integrated metamorphic and geochronologic data indicate rapid cooling of
693 the Inner Lesser Himalaya before 6 Ma, following peak metamorphism around 10 Ma [*Caddick*
694 *et al.*, 2007; *Thiede et al.*, 2009]}. We note that rapid cooling does not however require
695 synchronous unroofing. The first major flux of Himalayan zircons to the submarine fan is dated
696 at 7.99 to 7.78 Ma, although widespread Himalayan unroofing may not have started until 5.72
697 Ma, followed by Inner Lesser Himalayan unroofing starting around 1.56 Ma. This timing is
698 younger than reconstructed by Colleps *et al.* [2018] who favor exposure of the Outer Lesser
699 Himalaya after 16 Ma and of the Inner Lesser Himalaya after 11 Ma, although that study was
700 again located in an area father east, within the wetter Ganges catchment, and need not apply to
701 the drier Indus basin. A more erosive climate further east might favor earlier unroofing in that
702 area. The erosion data support the concept of significant along strike diachroneity of unroofing.

703 Uplift of the Lesser Himalayan Duplex would have created a topographic barrier,
704 susceptible to erosion as monsoon rains were focused along this topographic front. The
705 increasing Himalayan character of the total zircon input comes at a time when the summer
706 monsoon rains were generally weakening after ~8 Ma [*Dettman et al.*, 2001], or after 7.7 Ma
707 based on new environmental data from Site U1456 [*Clift et al.*, 2019a](Fig. 13). Moisture
708 delivery to this area from the winter westerlies has also been shown to have reduced around 7
709 Ma [*Vögeli et al.*, 2017]. In the recent geologic past, since the LGM, strong Himalayan rather
710 than Karakoram erosion has occurred when the summer monsoon was strong, during interglacial
711 times and not when it was weak during glacial times [*Clift et al.*, 2008a]. The increase in
712 Himalayan erosion over longer periods of time, correlating with the weakening monsoon, is the
713 opposite of this shorter-term trend. It is possible that solid Earth tectonic forces, rather than
714 climate, have dominated the long-term evolution of erosion, although the temporal correlation of
715 provenance and aridity is suggestive of a climatic control.

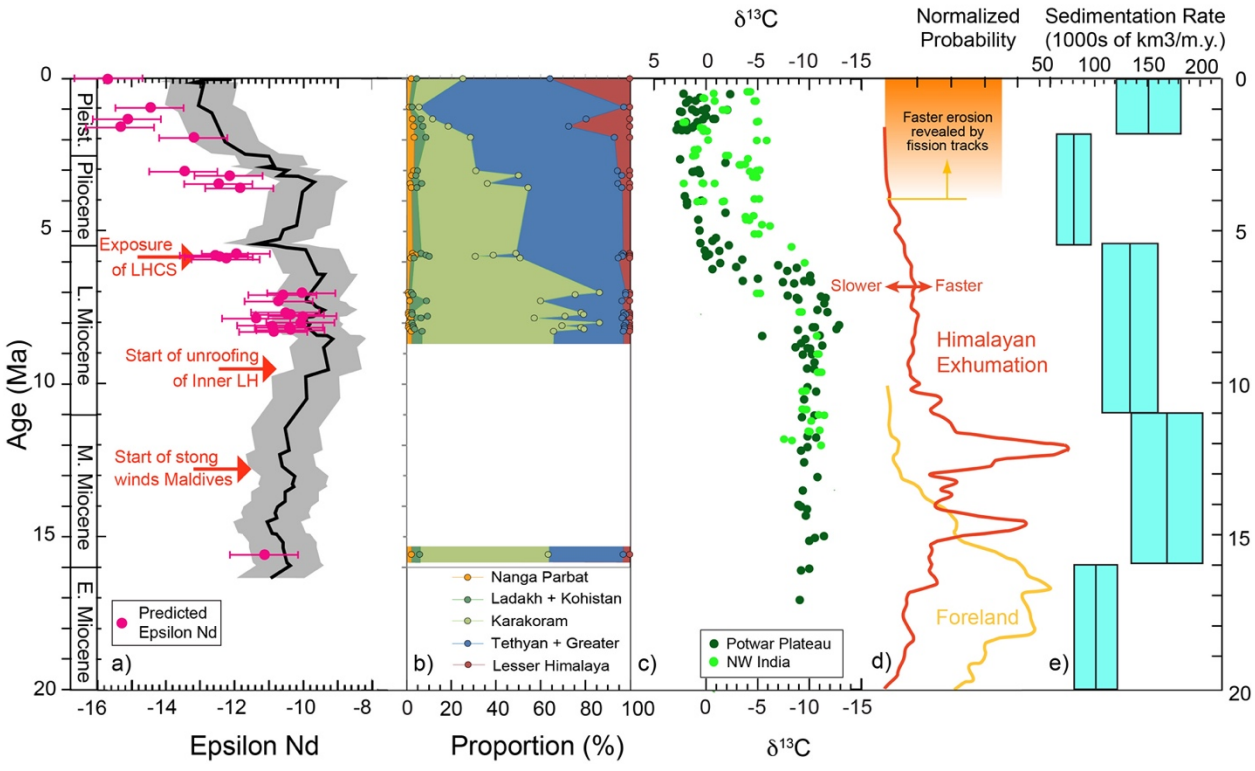

Figure 13. Comparison of climate, erosion and exhumation proxies in the Himalaya. (a) Smoothed Nd isotope history for the Indus River with grey background showing effective uncertainties from Clift *et al.* [2018]. (b) Breakdown of the sources of detrital zircons based on the unmixing procedure of Sundell and Saylor [2017]. (c) Carbon isotope character of pedogenic carbonate in Pakistan as an indicator of dominant vegetation in the Potwar Plateau of Pakistan [Quade *et al.*, 1989], and NW India [*Singh et al.*, 2011]. (d) Relative exhumation rates of the Greater Himalaya tracked by bedrock Ar-Ar dating [*Clift et al.*, 2008b] and zircon fission track from foreland basin sediment [Chirouze *et al.*, 2015]. (e) Rates of sediment supply to the Arabian Sea calculated from regional seismic [*Clift*, 2006].

All of the samples show the presence of very young zircons (<25 Ma) that possibly correlate with bedrock dates from Nanga Parbat, although these are never very numerous. It is also possible that some of these young ages may in fact be derived from erosion of fast exhuming rocks in parts of the southern Karakoram [*Wallis et al.*, 2014]. However, even if that this material was derived from Nanga Parbat, the low abundance of such zircon grains in the Laxmi Basin sediments would suggest that this massif was not generating very high proportions of sediment in the trunk Indus river, unlike the situation in the eastern syntaxis [*Garzanti et al.*, 2004; *Stewart et al.*, 2008]. This is consistent with the U-Pb zircon ages in the modern Indus River downstream of Nanga Parbat [*Alizai et al.*, 2011] that show neither many <25 Ma zircons or older 1500–2300 Ma grains that would be associated with less deeply buried rocks but with the Lesser Himalayan affiliation typically made with Nanga Parbat [*Whittington et al.*, 1999].

We compare our detrital zircon budget with that of the Nd budget published by Clift *et al.* [2019b]. Translating zircon budgets into rock erosion budgets is not easy due to bedrock zircon fertility variations. However, whole-rock geochemical analysis of Alizai *et al.* [2012] suggested that on average the eastern, Himalaya-draining tributaries are around 2.2 times more fertile in zircon than the trunk Indus. If we simply use the source percentages from the zircon unmixing calculation described above and the average ε_{Nd} values for these different units then it is possible to predict the average composition of the bulk sediment through time. We use an ε_{Nd} value of -14.6 for the Greater and Tethyan Himalaya, -21.7 for the Lesser Himalaya, -9.3 for the Karakoram, -20 for Nanga Parbat and +5.1 for Kohistan and the Transhimalaya based on synthesis of the bedrock data, but especially the composition of river sediments that are derived from wide areas of these ranges [*Clift et al.*, 2002b]. Transhimalaya Nd data are from Rolland *et al.* [2002], Singh *et al.* [2002], and Khan *et al.* [1997]. Greater and Lesser Himalayan data are from Ahmad *et al.* [2000], Deniel *et al.* [1987], Inger *et al.* [1993] and Parrish and Hodges [1996]. Karakoram data are from Crawford and Searle [1992] and Schärer *et al.* [1990].

The results of this estimate are shown next to the smoothed long-term Nd isotope evolution from bulk sediment analysis [*Clift et al.*, 2019b] (Fig. 13). We account for the ± 1 ε_{Nd} uncertainty value estimated from the Indus Quaternary [*Jonell et al.*, 2018]. We note that before 6 Ma the estimates overlap with the bulk sediment record that was derived from muddy lithologies, suggesting similar sources. After this time both the estimated and measured ε_{Nd} values became more negative. However, the predicted Nd isotope compositions are always more negative than those measured from the bulk sediment and this implies an over estimation in the flux from isotopically negative sources, i.e. the Himalaya, using the zircon method. This is consistent with the geochemical data indicating that the Himalaya are more abundant in zircon than the Karakoram, but have similar concentrations in Nd [*Alizai et al.*, 2011]. As a result, our zircon budget (Fig. 13) represents an overestimate of the influence of the Himalaya compared the Karakoram through time in terms of total rock eroded. Nonetheless, the overall trends in the two data sets are consistent and the reconstruction of increasing Himalayan erosion since the 5.72 Ma may be considered robust.

7. Conclusions

Sandy and silty sediments recovered from the Laxmi Basin in the Eastern Arabian Sea provide a relatively continuous erosional record derived from the Indus River and spanning the last 15.5 m.y. In this study samples were taken from IODP Sites U1456 and U1457 for geochemical and geochronological analyses. Detrital zircon grains were dated by U-Pb methods to determine their provenance. The sediments themselves are defined as wackes and are relatively immature in composition, with bulk sediment characters similar to those found in the Quaternary delta of the Indus and in its submarine Canyon. They are readily distinguishable from sediments on the Western Indian Shelf, confirming their derivation from the Indus River and not the peninsula with one exception. The sediments are mostly of silty sand to silt size, with only a few being classified as fine sand. Although the sediments are relatively depleted in Ca, Na and P relative to the upper continental crust this reflects chemical weathering during transport and does not affect the provenance analysis conducted here.

Detrital zircon U-Pb ages fall into a number of categories which can be correlated with bedrock sources in the Himalaya. The ubiquitous presence of zircon grains younger than 200 Ma requires the sediments to be the erosional products of the Himalaya/Karakoram and not peninsular India. The progressive increase in zircon grains dating at 350–1250 Ma, as well as 1500–2300 Ma, indicates that the erosional flux from the Himalaya increased through the studied time interval. Almost all the samples contain grains that could be derived from the Karakoram or from Kohistan, and there is an appearance of very young zircon grains, younger than 25 Ma, that is especially marked since 3.17 Ma. Such young zircon grains may be from Nanga Parbat or parts of the eastern Karakoram. Statistical analysis shows that there are a number of groupings and an increase in Himalayan erosion through time. High flux from the Himalaya was noted at 7.99–7.78 Ma and starting between 7.0 and 5.87 Ma. Since 1.32 Ma the sediments are similar to the modern Indus River, but not like the glacial-era river, which has more similarities with the Miocene Laxmi Basin samples and with enhanced erosion in the Karakoram. Detrital zircon population unmixing techniques allow us to objectively confirm the progressive increase of Himalayan erosion relative to the Karakoram, and the sharp jump in erosion from the Inner Lesser Himalayas starting at 1.56 Ma. This is somewhat younger than the anticipated unroofing of these ranges derived from earlier foreland studies, although much of the earlier data comes from further east in the Ganges catchment. The shift to more Himalayan erosion through time occurs as the monsoon climate weakened, as well as when the Lesser Himalayan Duplex formed. This suggests that the changing patterns of erosion could be largely a function of solid Earth tectonic forces building topography, although the correlation of unroofing to the Late Miocene drying trend does raise the possible role for climate too, albeit in the opposite fashion to that seen since the LGM, when more Himalayan erosion correlates with strong summer monsoon rains.

Acknowledgments

This study was made possible by samples provided by International Ocean Discovery Program (IODP). The work was partially funded by a grant from USSSP, as well as additional funding from the Charles T. McCord Chair in petroleum geology at LSU, and the Chevron (Gulf) Centennial professorship and the UTChron Laboratory at the University of Texas. We also would like to acknowledge Lisa Stockli for assistance with zircon U-Pb data acquisition and reduction. Data related to this study are available as tables within the article and from Mendeley (data.mendeley.com) at DOI: 10.17632/b57z79m4kj.1.

812 **References**

813 Ahmad, T., N. Harris, M. Bickle, H. Chapman, J. Bunbury, and C. Prince (2000), Isotopic
814 constraints on the structural relationships between the Lesser Himalayan Series and the
815 High Himalayan Crystalline Series, Garhwal Himalaya, *Geol. Soc. Am. Bull.*, *112*(3), 467-
816 477.
817 Alizai, A., A. Carter, P. D. Clift, S. VanLaningham, J. C. Williams, and R. Kumar (2011),
818 Sediment provenance, reworking and transport processes in the Indus River by U-Pb dating
819 of detrital zircon grains, *Global Planet. Change*, *76*, 33-55,
820 doi:10.1016/j.gloplacha.2010.11.008.
821 Alizai, A., S. Hillier, P. D. Clift, and L. Giosan (2012), Clay mineral variations in Holocene
822 terrestrial sediments from the Indus Basin; a response to SW Asian Monsoon variability,
823 *Quat. Res.*, *77*(3), 368–381, doi:10.1016/j.yqres.2012.01.008.
824 Amidon, W. H., D. W. Burbank, and G. E. Gehrels (2005), U-Pb zircon ages as a sediment
825 mixing tracer in the Nepal Himalaya, *Earth Planet. Sci. Letts.*, *235*(1-2), 244-260.
826 Baral, U., D. Lin, and D. Chamlagain (2015), Detrital zircon U–Pb geochronology of the Siwalik
827 Group of the Nepal Himalaya: implications for provenance analysis, *Intern. J. Earth Sci.*,
828 1-19, doi;10.1007/s00531-015-1198-7.
829 Bernet, M., P. van der Beek, R. Pik, P. Huyghe, J.-L. Mugnier, E. Labrin, et al. (2006), Miocene
830 to Recent exhumation of the central Himalaya determined from combined detrital zircon
831 fission-track and U/Pb analysis of Siwalik sediments, western Nepal, *Basin Res.*, *18*, 393–
832 412, doi: 10.1111/j.1365-2117.2006.00303.
833 Bhattacharya, G. C. B., A. K. Chaubey, G. P. S. Murty, S. Srinivas, K. V. Sarma, V.
834 Subrahmanyam, et al. (1994), Evidence for seafoor spreading in the Laxmi Basin,
835 northeastern Indian Ocean, *Earth Planet. Sci. Letts.*, *125*, 211-220.
836 Bollinger, L., J. P. Avouac, O. Beyssac, E. J. Catlos, T. M. Harrison, M. Grove, et al. (2004),
837 Thermal structure and exhumation history of the Lesser Himalaya in central Nepal,
838 *Tectonics*, *23*(5), 19, doi:10.1029/2003TC001564.
839 Bookhagen, B., R. C. Thiede, and M. R. Strecker (2005), Late Quaternary intensified monsoon
840 phases control landscape evolution in the northwest Himalaya, *Geology*, *33*(2), 149-152,
841 doi:10.1130/G20982.1.
842 Burbank, D. W., A. E. Blythe, J. Putkonen, B. Pratt-Sitaula, E. Gabet, M. Oskins, et al. (2003),
843 Decoupling of erosion and precipitation in the Himalayas, *Nature*, *426*, 652–655.
844 Caddick, M. J., M. J. Bickle, N. B. W. Harris, T. J. B. Holland, M. S. A. Horstwood, R. R.
845 Parrish, et al. (2007), Burial and exhumation history of a Lesser Himalayan schist:
846 Recording the formation of an inverted metamorphic sequence in NW India, *Earth Planet.*
847 *Sci. Letts.*, *264*(3–4), 375–390, doi:10.1016/j.epsl.2007.09.011.
848 Caley, T., D. M. Roche, and H. Renssen (2014), Orbital Asian summer monsoon dynamics
849 revealed using an isotope-enabled global climate model, *Nature Comm.*, *5*, 5371,
850 doi:10.1038/ncomms6371.
851 Calvès, G., M. Huuse, P. D. Clift, and S. Brusset (2015), Giant fossil mass wasting off the coast
852 of West India: The Nataraja submarine slide, *Earth Planet. Sci. Letts.*, *432*, 265–272,
853 doi:10.1016/j.epsl.2015.10.022.
854 Catlos, E. J., T. M. Harrison, M. J. Kohn, M. Grove, F. J. Ryerson, C. E. Manning, et al. (2001),
855 Geochronologic and thermobarometric constraints on the evolution of the Main Central
856 Thrust, central Nepal Himalaya, *J. Geophys. Res.*, *106*(B8), 16,177-116,204.

857 Chirouze, F., P. Huyghe, C. Chauvel, P. van der Beek, M. Bernet, and J.-L. Mugnier (2015),
858 Stable Drainage Pattern and Variable Exhumation in the Western Himalaya since the
859 Middle Miocene, *J. Geol.*, *123*, 1–20, doi:10.1086/679305.
860 Clift, P., C. Gaedicke, R. Edwards, J. Lee, II, P. Hildebrand, S. Amjad, et al. (2002a), The
861 stratigraphic evolution of the Indus Fan and the history of sedimentation in the Arabian
862 Sea, *Mar. Geophys. Res.*, *23*(3), 223-245.
863 Clift, P. D. (2006), Controls on the erosion of Cenozoic Asia and the flux of clastic sediment to
864 the ocean, *Earth Planet. Sci. Letts.*, *241*(3-4), 571-580.
865 Clift, P. D., and J. S. Blusztajn (2005), Reorganization of the western Himalayan river system
866 after five million years ago, *Nature*, *438*(7070), 1001-1003.
867 Clift, P. D., I. H. Campbell, M. S. Pringle, A. Carter, X. Zhang, K. V. Hodges, et al. (2004),
868 Thermochronology of the modern Indus River bedload; new insight into the control on the
869 marine stratigraphic record, *Tectonics*, *23*(TC5013), doi:10.1029/2003TC001559.
870 Clift, P. D., L. Giosan, J. Blusztajn, I. H. Campbell, C. M. Allen, M. Pringle, et al. (2008a),
871 Holocene erosion of the Lesser Himalaya triggered by intensified summer monsoon,
872 *Geology*, *36*(1), 79–82, doi: 10.1130/G24315A.1.
873 Clift, P. D., L. Giosan, A. Carter, E. Garzanti, V. Galy, A. R. Tabrez, et al. (2010), Monsoon
874 control over erosion patterns in the Western Himalaya: possible feed-backs into the
875 tectonic evolution, in *Monsoon evolution and tectonic-climate linkage in Asia*, edited by P.
876 D. Clift, R. Tada and H. Zheng, pp. 181–213, Geological Society, London.
877 Clift, P. D., K. Hodges, D. Heslop, R. Hannigan, L. V. Hoang, and G. Calves (2008b), Greater
878 Himalayan exhumation triggered by Early Miocene monsoon intensification, *Nature*
879 *Geosci.*, *1*, 875-880, doi:10.1038/ngeo351.
880 Clift, P. D., D. K. Kulhanek, P. Zhou, M. G. Bowen, S. M. Vincent, M. Lyle, et al. (2019a),
881 Chemical Weathering and Erosion Responses to Changing Monsoon Climate in the Late
882 Miocene of Southwest Asia, *Geol. Mag.*, doi:10.1017/S0016756819000608.
883 Clift, P. D., J. I. Lee, P. Hildebrand, N. Shimizu, G. D. Layne, J. Blusztajn, et al. (2002b), Nd
884 and Pb isotope variability in the Indus River system; implications for sediment provenance
885 and crustal heterogeneity in the western Himalaya, *Earth Planet. Sci. Letts.*, *200*(1-2), 91-
886 106, doi:10.1016/S0012-821X(02)00620-9.
887 Clift, P. D., N. Shimizu, G. Layne, C. Gaedicke, H. U. Schlüter, M. K. Clark, et al. (2001),
888 Development of the Indus Fan and its significance for the erosional history of the western
889 Himalaya and Karakoram, *Geol. Soc. Am. Bull.*, *113*, 1039–1051.
890 Clift, P. D., P. Zhou, D. F. Stockli, and J. Blusztajn (2018), Regional Pliocene Exhumation of the
891 Lesser Himalaya in the Indus Drainage, *Solid Earth*, doi:10.5194/se-2018-132.
892 Clift, P. D., P. Zhou, D. F. Stockli, and J. Blusztajn (2019b), Regional Pliocene Exhumation of
893 the Lesser Himalaya in the Indus Drainage, *Solid Earth*, *10*, 647–661, doi:10.5194/se-10-
894 647-2019.
895 Colleps, C. L., R. N. McKenzie, D. F. Stockli, N. C. Hughes, B. P. Singh, A. A. G. Webb, et al.
896 (2018), Zircon (U-Th)/He thermochronometric constraints on Himalayan thrust belt
897 exhumation, bedrock weathering, and Cenozoic seawater chemistry, *Geochem. Geophys.*
898 *Geosyst.*, *19*, 257– 271, doi:10.1002/2017GC007191.
899 Colleps, C. L., D. F. Stockli, N. R. McKenzie, A. G. Webb, and B. K. Horton (2019), Neogene
900 kinematic evolution and exhumation of the NW India Himalaya: Zircon geo-
901 /thermochronometric insights from the fold-thrust belt and foreland basin, *Tectonics*, *38*,
902 2059–2086, 10.1029/2018TC005304.

903 Courtillot, V., Y. Gallet, R. Rocchia, G. Féraud, E. Robin, C. Hofmann, et al. (2000), Cosmic
904 markers, 40Ar/39Ar dating and paleomagnetism of the KT sections in the Anjar Area of
905 the Deccan large igneous province, *Earth Planet. Sci. Letts.*, *182*, 137-156.
906 Crawford, M. B., and M. P. Searle (1992), Field relationships and geochemistry of pre-
907 collisional (India-Asia) granitoid magmatism in the central Karakoram, northern Pakistan,
908 *Tectonophysics*, *206*(1-2), 171-192.
909 Dailey, S. K., P. D. Clift, D. K. Kulhanek, J. Blusztajn, C. M. Routledge, G. Calvès, et al.
910 (2019), Large-scale Mass Wasting on the Miocene Continental Margin of Western India,
911 *Geol. Soc. Am. Bull.*, doi:/10.1130/B35158.1.
912 DeCelles, P. G., G. E. Gehrels, Y. Najman, A. J. Martin, A. Carter, and E. Garzanti (2004),
913 Detrital geochronology and geochemistry of Cretaceous-Early Miocene strata of Nepal:
914 implications for timing and diachroneity of initial Himalayan orogenesis, *Earth Planet. Sci.*
915 *Letts.*, *227*(3-4), 313-330.
916 DeCelles, P. G., G. E. Gehrels, J. Quade, B. LaReau, and M. Spurlin (2000), Tectonic
917 implications of U-Pb zircon ages of the Himalayan orogenic belt in Nepal, *Science*,
918 *288*(5465), 497-499, doi:10.1126/science.288.5465.497.
919 Deniel, C., P. Vidal, A. Fernandez, P. Fort, and J.-J. Peucat (1987), Isotopic study of the Manaslu
920 granite (Himalaya, Nepal): inferences on the age and source of Himalayan leucogranites,
921 *Contribs. Min. Petrol.*, *96*(1), 78-92.
922 Deptuck, M. E., D. J. Piper, B. Savoye, and A. Gervais (2008), Dimensions and architecture of
923 late Pleistocene submarine lobes off the northern margin of East Corsica, *Sedimentology*,
924 *55*(4), 869-898.
925 Dettman, D. L., M. J. Kohn, J. Quade, F. J. Ryerson, T. P. Ojha, and S. Hamidullah (2001),
926 Seasonal stable isotope evidence for a strong Asian monsoon throughout the past 10.7 m.y,
927 *Geology*, *29*(1), 31-34.
928 Dunlap, W. J., and R. Wysoczanski (2002), Thermal evidence for Early Cretaceous
929 metamorphism in the Shyok suture zone and age of the Khardung volcanic rocks, Ladakh,
930 India, *J. Asian Earth Sci.*, *20*(5), 481-490.
931 Dunlea, A. G., R. W. Murray, J. Sauvage, A. J. Spivack, R. N. Harris, and S. D'Hondt (2015),
932 Dust, volcanic ash, and the evolution of the South Pacific Gyre through the Cenozoic,
933 *Paleocean.*, *30*(8), 1078-1099, doi:10.1002/2015PA002829.
934 Fedo, C. M., H. W. Nesbitt, and G. M. Young (1995), Unraveling the effects of potassium
935 metasomatism in sedimentary rocks and paleosols, with implications for paleoweathering
936 conditions and provenance, *Geology*, *23*, 921–924.
937 Fleitmann, D., S. J. Burns, M. Mudelsee, U. Neff, J. Kramers, A. Mangini, et al. (2003),
938 Holocene forcing of the Indian monsoon recorded in a stalagmite from southern Oman,
939 *Science*, *300*(5626), 1737-1739.
940 Folk, R. L. (1974), *Petrology of Sedimentary Rocks*, 182 pp., Hemphill Press, Austin, Texas.
941 Fraser, J. E., M. P. Searle, R. R. Parrish, and S. R. Noble (2001), Chronology of deformation,
942 metamorphism, and magmatism in the southern Karakoram Mountains, *Geol. Soc. Am.*
943 *Bull.*, *113*(11), 1443-1455.
944 Gaedicke, C., H.-U. Schlueter, H.-A. Roeser, A. Prexl, B. Schreckenberger, H. Meyer, et al.
945 (2002), Origin of the northern Indus Fan and Murray Ridge, northern Arabian Sea;
946 interpretation from seismic and magnetic imaging, *Tectonophysics*, *355*, 127-143.
947 Garzanti, E., S. Andò, and G. Vezzoli (2009), Grain-size dependence of sediment composition
948 and environmental bias in provenance studies, *Earth Planet. Sci. Letts.*, *277*(3-4), 422-432.

949 Garzanti, E., A. Baud, and G. Mascle (1987), Sedimentary record of the northward flight of India
950 and its collision with Eurasia (Ladakh Himalaya, India), *Geodin. Acta*, *1*(4/5), 297–312.
951 Garzanti, E., W. Liang, S. Andò, P. D. Clift, A. Resentini, P. Vermeesch, et al. (2020),
952 Provenance of Thal Desert sand: Focused erosion in the western Himalayan syntaxis and
953 foreland-basin deposition driven by latest Quaternary climate change, *Earth Sci. Rev.*, *207*,
954 103220, doi:10.1016/j.earscirev.2020.103220.
955 Garzanti, E., G. Vezzoli, S. Ando, C. France-Lanord, S. K. Singh, and G. Foster (2004), Sand
956 petrology and focused erosion in collision orogens: the Brahmaputra case, *Earth Planet.*
957 *Sci. Letts.*, *220*(1-2), 157-174.
958 Garzanti, E., G. Vezzoli, S. Ando, P. Paparella, and P. D. Clift (2005), Petrology of Indus River
959 sands; a key to interpret erosion history of the western Himalayan syntaxis, *Earth Planet.*
960 *Sci. Letts.*, *229*(3-4), 287-302, doi: 10.1016/j.epsl.2004.11.008.
961 Gehrels, G. (2012), Detrital Zircon U‐Pb Geochronology: Current Methods and New
962 Opportunities, in *Tectonics of Sedimentary Basins*, edited by C. Busby and A. Azor, pp.
963 47-62, Wiley, doi:10.1002/9781444347166.ch2.
964 Gehrels, G. E., P. Kapp, P. DeCelles, A. Pullen, R. Blakely, A. Weislgel, et al. (2011), Detrital
965 zircon geochronology of pre-Tertiary strata in the Tibetan-Himalayan orogen, *Tectonics*,
966 *30*(TC5016), doi:10.1029/2011TC002868.
967 Gehrels, G. E., V. Valencia, and J. Ruiz (2008), Enhanced precision, accuracy, efficiency, and
968 spatial resolution of U-Pb ages by laser ablation–multicollector–inductively coupled
969 plasma–mass spectrometry, *Geochem. Geophys. Geosyst.*, *9*(Q03017),
970 doi:10.1029/2007GC001805.
971 Guidry, M. W., and F. T. Mackenzie (2000), Apatite weathering and the Phanerozoic phosphorus
972 cycle, *Geology*, *28*(7), 631-634.
973 Gupta, A. K., D. M. Anderson, and J. T. Overpeck (2003), Abrupt changes in the Asian
974 southwest monsoon during the Holocene and their links to the North Atlantic Ocean,
975 *Nature*, *421*, 354–356.
976 Hart, N. R., D. F. Stockli, and N. W. Hayman (2016), Provenance evolution during progressive
977 rifting and hyperextension using bedrock and detrital zircon U-Pb geochronology, Mauléon
978 Basin, western Pyrenees, *Geosphere*, *12*(4), 1166-1186, doi:10.1130/GES01273.1.
979 Herron, M. M. (1988), Geochemical classification of terrigenous sands and shales from core or
980 log data, *J. Sed. Petrol.*, *58*, 820–829.
981 Hildebrand, P. R., S. R. Noble, M. P. Searle, D. J. Waters, and R. R. Parrish (2001), Old origin
982 for an active mountain range; geology and geochronology of the eastern Hindu Kush,
983 Pakistan, *Geol. Soc. Am. Bull.*, *113*(5), 625-639.
984 Hodges, K. (2003), Geochronology and thermochronology in orogenic systems, in *The Crust*,
985 edited by R. Rudnick, pp. 263-292, Elsevier-Science, Amsterdam.
986 Hodges, K. V. (2000), Tectonics of the Himalaya and southern Tibet from two perspectives,
987 *Geol. Soc. Am. Bull.*, *112*(3), 324-350.
988 Honegger, K., V. Dietrich, W. Frank, A. Gansser, M. Thoni, and V. F. Trommsdorf (1982),
989 Magmatism and metamorphism in the Ladakh Himalayas (The Indus-Tsangpo suture
990 zone), *Earth Planet. Sci. Letts.*, *60*, 178-194.
991 Howell, A. L., S. J. Bentley, K. Xu, R. E. Ferrell, Z. Muhammad, and E. Septama (2014), Fine
992 sediment mineralogy as a tracer of latest Quaternary sediment delivery to a dynamic
993 continental margin: Pandora Trough, Gulf of Papua, Papua New Guinea, *Mar. Geol.*, *357*,
994 108-122, doi:10.1016/j.margeo.2014.08.003.

Hu, X., E. Garzanti, J. Wang, W. Huang, W. An, and A. Webb (2016), The timing of India-Asia collision onset – Facts, theories, controversies, *Earth Sci. Rev.*, *160*, 264-299, doi:10.1016/j.earscirev.2016.07.014.

Huyghe, P., A. Galy, J.-L. Mugnier, and C. France-Lanord (2001), Propagation of the thrust system and erosion in the Lesser Himalaya: Geochemical and sedimentological evidence, *Geology*, *29*(11), 1007–1010.

Inger, S., and N. Harris (1993), Geochemical constraints on leucogranite magmatism in the Langtang Valley, Nepal Himalaya, *J. Petrol.*, *34*(2), 345-368.

Jackson, S. E., N. J. Pearson, W. L. Griffin, and E. A. Belousova (2004), The application of laser ablation-inductively coupled plasma-mass spectrometry (LA-ICP-MS) to in situ U–Pb zircon geochronology, *Chem. Geol.*, *211*, 47–69.

Jaeger, J.-J., V. Courtillot, and P. Tapponnier (1989), Paleontological view of the ages of the Deccan Traps, the Cretaceous/Tertiary boundary, and the India-Asia collision, *Geology*, *17*(4), 316-319, doi:10.1130/0091-7613(1989)017<0316:Pvotao>2.3.Co;2.

Jonell, T. N., A. Carter, P. Böning, K. Pahnke, and P. D. Clift (2017), Climatic and glacial impact on erosion patterns and sediment provenance in the Himalayan rain shadow, Zanskar River, NW India, *Geol. Soc. Am. Bull.*, *129*(7-8), 820-836, doi:10.1130/B31573.

Jonell, T. N., Y. Li, J. Blusztajn, L. Giosan, and P. D. Clift (2018), Signal or noise? Isolating grain size effects on Nd and Sr isotope variability in Indus delta sediment provenance, *Chem. Geol.*, *485*, 56–73, doi:10.1016/j.chemgeo.2018.03.036.

Khan, M. A., R. J. Stern, R. F. Gribble, and B. F. Windley (1997), Geochemical and isotopic constraints on subduction polarity, magma sources, and palaeogeography of the Kohistan intra-oceanic arc, northern Pakistan Himalaya, *J. Geol. Soc.*, *154*, 935–946.

Khim, B.-K., K. Horikawa, Y. Asahara, J.-E. Kim, and M. Ikehara (2019), Detrital Sr-Nd isotopes, sediment provenances, and depositional processes in the Laxmi Basin of the Arabian Sea during the last 800 kyrs, *Geol. Mag.*, 1-13, doi:10.1017/S0016756818000596.

Klootwijk, C. T., J. S. Gee, J. W. Peirce, G. M. Smith, and P. L. McFadden (1992), An early India-Asia contact: Paleomagnetic constraints from Ninetyeast Ridge, ODP Leg 121, *Geology*, *20*(5), 395-398, DOI: 10.1130/0091-7613(1992)020.

Kolla, V., and F. Coumes (1987), Morphology, internal structure, seismic stratigraphy, and sedimentation of Indus Fan, *AAPG Bull.*, *71*, 650–677.

Krol, M. A., P. K. Zeitler, and P. Copeland (1996), Episodic unroofing of the Kohistan Batholith, Pakistan: Implications from K-feldspar thermochronology, *J. Geophys. Res.-Solid Earth*, *101*(B12), 28149-28164.

Kurian, S., B. N. Nath, N. C. Kumar, and K. K. C. Nair (2013), Geochemical and Isotopic Signatures of Surficial Sediments from the Western Continental Shelf of India: Inferring Provenance, Weathering, and the Nature of Organic Matter Geochemical and Isotopic Signatures of Sediments From The Indian West Coast, *J. Sed. Res.*, *83*(6), 427-442, doi:10.2110/jsr.2013.36.

Lavé, J., and J. P. Avouac (2000), Active folding of fluvial terraces across the Siwaliks Hills (Himalayas of central Nepal), *J. Geophys. Res.*, *105*, 5735–5770, doi: 10.1029/1999JB900292.

Lawrence, R. L., R. Cox, R. W. Mapes, and D. S. Coleman (2011), Hydrodynamic fractionation of zircon age populations, *GSA Bulletin*, *123*(1-2), 295-305, doi:10.1130/B30151.1.

Le Fort, P., F. Debon, and J. Sonet (1983), Petrography, geochemistry and geochronology of some samples from the Karakoram Batholith (N. Pakistan), in *Granites of the Himalayas,*

Karakoram and Hindu Kush, edited by F. A. Shams, pp. 377–387, Punjab University, Lahore, Pakistan.

Li, Y., P. D. Clift, P. Böning, J. Blusztajn, R. W. Murray, T. Ireland, et al. (2018), Continuous Signal Propagation in the Indus Submarine Canyon since the Last Deglacial, *Mar. Geol.*, *406*, 159–176, doi:10.1016/j.margeo.2018.09.011.

Li, Y., P. D. Clift, and P. O'Sullivan (2019), Millennial and Centennial Variations in Zircon U-Pb and Apatite Fission Track Ages in the Quaternary Indus Submarine Canyon, *Basin Res.*, *31*, 155–170, doi:10.1111/bre.12313.

Malusà, M. G., A. Resentini, and E. Garzanti (2016), Hydraulic sorting and mineral fertility bias in detrital geochronology, *Gondwana Res.*, *31*, 1-19, doi:10.1016/j.gr.2015.09.002.

Marsh, A. D., W. G. Parker, D. F. Stockli, and J. W. Martz (2019), Regional correlation of the Sonsela Member (Upper Triassic Chinle Formation) and detrital U-Pb zircon data from the Sonsela Sandstone bed near the Sonsela Buttes, northeastern Arizona, USA, support the presence of a distributive fluvial system, *Geosphere*, *15*(4), 1128-1139, doi:10.1130/GES02004.1.

Marsh, J. H., and D. F. Stockli (2015), Zircon U–Pb and trace element zoning characteristics in an anatectic granulite domain: Insights from LASS-ICP-MS depth profiling, *Lithos*, *239*, 170-185, doi:10.1016/j.lithos.2015.10.017.

Molnar, P. (2001), Climate change, flooding in arid environments, and erosion rates, *Geology*, *29*(12), 1071-1074.

Mukhopadhyay, G., S. Mukhopadhyay, M. Roychowdhury, and P. Parui (2010), Stratigraphic correlation between different Gondwana basins of India, *J. Geol. Soc. India*, *76*(3), 251-266.

Myrow, P. M., N. C. Hughes, L. A. Derry, R. N. McKenzie, G. Jiang, A. A. G. Webb, et al. (2015), Neogene marine isotopic evolution and the erosion of Lesser Himalayan strata: Implications for Cenozoic tectonic history, *Earth Planet. Sci. Letts.*, *417*, 142-150, doi:10.1016/j.epsl.2015.02.016.

Najman, Y. (2006), The detrital record of orogenesis: A review of approaches and techniques used in the Himalayan sedimentary basins, *Earth Sci. Rev.*, *74*(1-2), 1-72.

Najman, Y., E. Appel, M. Boudagher‐Fadel, P. Bown, A. Carter, E. Garzanti, et al. (2010), Timing of India‐Asia collision: Geological, biostratigraphic, and palaeomagnetic constraints, *J. Geophys. Res.*, *115*(B12416), doi:10.1029/2010JB007673.

Najman, Y., M. Bickle, E. Garzanti, M. Pringle, D. Barfod, N. Brozovic, et al. (2009), Reconstructing the exhumation history of the Lesser Himalaya, NW India, from a multitechnique provenance study of the foreland basin Siwalik Group, *Tectonics*, *28*(TC5018), doi:10.1029/2009TC002506.

Najman, Y., D. Jenks, L. Godin, M. Boudagher-Fadel, I. Millar, E. Garzanti, et al. (2017), The Tethyan Himalayan detrital record shows that India–Asia terminal collision occurred by 54 Ma in the Western Himalaya, *Earth Planet. Sci. Letts.*, *459*, 301-310, doi:10.1016/j.epsl.2016.11.036.

Nesbitt, H. W., G. Markovics, and R. C. Price (1980), Chemical processes affecting alkalis and alkaline earths during continental weathering, *Geochim. Cosmochim. Acta*, *44*, 1659–1666.

Pandey, D. K., P. D. Clift, D. K. Kulhanek, S. Andò, J. A. P. Bendle, S. Bratenkov, et al. (2016a), Site U1456, in *Arabian Sea Monsoon. Proceedings of the International Ocean Discovery Program*, edited by D. K. Pandey, P. D. Clift and D. K. Kulhanek, International Ocean Discovery Program, College Station, TX, doi:10.14379/iodp.proc.355.103.2016.

Pandey, D. K., P. D. Clift, D. K. Kulhanek, S. Andò, J. A. P. Bendle, S. Bratenkov, et al. (2016b), Site U1457, in *Arabian Sea Monsoon. Proceedings of the International Ocean Discovery Program*, edited by D. K. Pandey, P. D. Clift and D. K. Kulhanek, International Ocean Discovery Program, College Station, TX, doi:10.14379/iodp.proc.355.104.2016.

Pandey, D. K., P. D. Clift, D. K. Kulhanek, and Expedition 355 Scientists (2016c), Arabian Sea Monsoon, *Proc. Int. Ocean Disc. Prog.*, *355*, doi:10.14379/iodp.proc.355.2016.

Pandey, D. K., P. D. Clift, D. K. Kulhanek, and Expedition 355 Scientists (2016d), Arabian Sea Monsoon: Expedition Summary, *Proc. Int. Ocean Disc. Prog.*, *355*, 1-32, doi:10.14379/iodp.proc.355.101.2016.

Pandey, O. P., P. K. Agrawal, and J. G. Negi (1995), Lithospheric structure beneath Laxmi Ridge and late Cretaceous geodynamic events, *Geo-Mar. Lett.*, *15*, 85-91.

Parrish, R. R., and K. V. Hodges (1996), Isotopic constraints on the age and provenance of the Lesser and Greater Himalayan sequences, Nepalese Himalaya, *Geol. Soc. Am. Bull.*, *108*(7), 904-911.

Parrish, R. R., and R. Tirrul (1989), U-Pb age of the Baltoro Granite, Northwest Himalaya, and implications for monazite U-Pb systematics, *Geology*, *17*, 1076–1079.

Paton, C., J. Hellstrom, B. Paul, J. Woodhead, and J. Hergt (2011), Iolite: Freeware for the visualisation and processing of mass spectrometric data, *J. Analyt. Atom. Spect.*, *26*(12), 2508–2518.

Petrus, J. A., and B. S. Kamber (2012), VizualAge: A novel approach to laser ablation ICP-MS U-Pb geochronology data reduction, *Geostand. Geoanalyt. Res.*, *36*(3), 247–270.

Quade, J., T. E. Cerling, and J. R. Bowman (1989), Development of Asian monsoon revealed by marked ecological shift during the latest Miocene in northern Pakistan, *Nature*, *342*(6246), 163-166.

Ravikant, V., F. Y. Wu, and W. Q. Ji (2009), Zircon U-Pb and Hf isotopic constraints on petrogenesis of the Cretaceous-Tertiary granites in eastern Karakoram and Ladakh, India, *Lithos*, *110*, 153-166.

Roddaz, M., A. Said, S. p. Guillot, P. O. Antoine, J. M. Montel, F. Martin, et al. (2011), Provenance of Cenozoic sedimentary rocks from the Sulaiman fold and thrust belt, Pakistan: implications for the palaeogeography of the Indus drainage system, *J. Geol. Soc.*, *168*, 499-516 doi: 10.1144/0016-76492010-100.

Rolland, Y., C. Picard, A. Pecher, H. Lapierre, D. Bosch, and F. Keller (2002), The Cretaceous Ladakh arc of NW himalaya—slab melting and melt–mantle interaction during fast northward drift of Indian Plate, *Chem. Geol.*, *182*, 139–178.

Routledge, C. M., D. K. Kulhanek, L. Tauxe, G. Scardia, A. D. Singh, S. Steinke, et al. (2019), Revised geological timescale for IODP Sites U1456 and U1457, *Geol. Mag.*, doi:10.1017/S0016756819000104.

Schärer, U., P. Copeland, T. M. Harrison, and M. P. Searle (1990), Age, cooling history, and origin of post-collisional leucogranites in the Karakoram Batholith; a multi-system isotope study, *J. Geol.*, *98*(2), 233-251.

Schärer, U., R.-H. Xu, and C. J. Allègre (1984), U-Pb geochronology of Gangdese (Transhimalaya) plutonism in the Lhasa-Xigaze region, Tibet, *Earth Planet. Sci. Letts.*, *69*(2), 311-320.

Searle, M. P. (1996), Cooling history, erosion, exhumation and kinematics of the Himalaya-Karakoram-Tibet orogenic belt, in *The Tectonic Evolution of Asia*, edited by A. Yin and T. M. Harrison, pp. 110-137, Cambridge University Press, Cambridge.

Searle, M. P., and R. J. Phillips (2007), Relationships between right-lateral shear along the Karakoram Fault and metamorphism, magmatism, exhumation and uplift; evidence from the K2-Gasherbrum-Pangong ranges, north Pakistan and Ladakh, *J. Geol. Soc.*, *164*(2), 439-450.

Searle, M. P., A. J. Rex, R. Tirrul, D. C. Rex, A. Barnicoat, and B. F. Windley (1989), Metamorphic, magmatic and tectonic evolution of the Central Karakoram in the Biafo-Baltoro-Hushe regions of north Pakistan, *Geol. Soc. America Spec. Pap.*, *232*, 47-73.

Shanmugam, G., and R. Moiola (1991), Types of submarine fan lobes: models and implications (1), *AAPG Bull.*, *75*(1), 156-179.

Shuaib, S. M. (1982), Geology and hydrocarbon potential of offshore Indus Basin, Pakistan, *AAPG Bull.*, *66*, 940–946.

Singh, S., R. Kumar, M. E. Barley, and A. K. Jain (2007), SHRIMP U–Pb ages and depth of emplacement of Ladakh batholith, eastern Ladakh, India, *J. Asian Earth Sci.*, *30*(3), 490–503.

Singh, S., B. Parkash, A. K. Awasthi, and S. Kumar (2011), Late Miocene record of palaeovegetation from Siwalik palaeosols of the Ramnagar sub-basin, India, *Current Sci.*, *100*(2), 213-222.

Singh, S. K., and C. France-Lanord (2002), Tracing the distribution of erosion in the Brahmaputra watershed from isotopic compositions of stream sediments, *Earth Planet. Sci. Letts.*, *202*(3-4), 645-662.

Spencer, C. J., C. L. Kirkland, and R. J. M. Taylor (2016), Strategies towards statistically robust interpretations of in situ U–Pb zircon geochronology, *Geoscience Frontiers*, *7*(4), 581-589, doi:10.1016/j.gsf.2015.11.006.

Stephenson, B. J., M. P. Searle, D. J. Waters, and D. C. Rex (2001), Structure of the Main Central Thrust zone and extrusion of the High Himalayan deep crustal wedge, Kishtwar-Zanskar Himalaya, *J. Geol. Soc.*, *158*(4), 637-652.

Stewart, R. J., B. Hallet, P. K. Zeitler, M. A. Malloy, C. M. Allen, and D. Trippett (2008), Brahmaputra sediment flux dominated by highly localized rapid erosion from the easternmost Himalaya, *Geology*, *36*(9), 711–714, doi: 10.1130/G24890A.1.

Sundell, K., and J. E. Saylor (2017), Unmixing detrital geochronology age distributions, *Geochem. Geophys. Geosyst.*, *18*, 2872–2886.

Taylor, S. R., and S. M. McLennan (1995), The geochemical evolution of the continental crust, *Rev. Geophys.*, *33*, 241–265.

Thiede, R. C., B. Bookhagen, J. R. Arrowsmith, E. R. Sobel, and M. R. Strecker (2004), Climatic control on rapid exhumation along the Southern Himalayan Front, *Earth Planet. Sci. Letts.*, *222*(3-4), 791-806.

Thiede, R. C., T. A. Ehlers, B. Bookhagen, and M. R. Strecker (2009), Erosional variability along the northwest Himalaya, *J. Geophys. Res.*, *114*(F01015), doi:10.1029/2008JF001010.

Vermeesch, P. (2004), How many grains are needed for a provenance study?, *Earth Planet. Sci. Letts.*, *224*, 351–441.

Vermeesch, P., A. Resentini, and E. Garzanti (2016), An R package for statistical provenance analysis, *Sed. Geol.*, *336*, 14-25, doi:10.1016/j.sedgeo.2016.01.009.

Vögeli, N., Y. Najman, P. van der Beek, P. Huyghe, P. M. Wynn, G. Govin, et al. (2017), Lateral variations in vegetation in the Himalaya since the Miocene and implications for climate evolution, *Earth Planet. Sci. Letts.*, *471*, 1–9, doi:10.1016/j.epsl.2017.04.037.

Wallis, D., A. Carter, R. J. Phillips, A. J. Parsons, and M. P. Searle (2016), Spatial variation in exhumation rates across Ladakh and the Karakoram: New apatite fission track data from the Eastern Karakoram, NW India, *Tectonics*, *35*, 704–721, doi:10.1002/2015TC003943.

Wallis, D., R. J. Phillips, and G. E. Lloyd (2014), Evolution of the Eastern Karakoram Metamorphic Complex, Ladakh, NW India, and its relationship to magmatism and regional tectonics, *Tectonophysics*, *626*, 41–52, doi:10.1016/j.tecto.2014.03.023.

Webb, A. A. G. (2013), Preliminary palinspastic reconstruction of Cenozoic deformation across the Himachal Himalaya (northwestern India), *Geosphere*, *9*, 572-587.

Weinberg, R. F., and W. J. Dunlap (2000), Growth and Deformation of the Ladakh Batholith, Northwest Himalayas: Implications for Timing of Continental Collision and Origin of Calc‐Alkaline Batholiths, *J. Geol.*, *108*, 303–320, DOI: 10.1086/314405.

Whipple, K. X. (2009), The influence of climate on the tectonic evolution of mountain belts *Nature Geosci.*, *2*, 1-8, doi: 10.1038/ngeo413.

White, A. F., and S. L. Brantley (1995), *Chemical weathering rates of silicate minerals*, 581 pp., Mineralogical Society of America.

Whittington, A., G. Foster, N. Harris, D. Vance, and M. Ayres (1999), Lithostratigraphic correlations in the western Himalaya - An isotopic approach, *Geology*, *27*(7), 585-588.

Wilson, S. A. (1997), Data compilation for USGS reference material BHVO-2, Hawaiian Basalt, *U.S. Geol. Surv. Open-File Rept*.

Wobus, C. W., K. V. Hodges, and K. X. Whipple (2003), Has focused denudation sustained active thrusting at the Himalayan topographic front?, *Geology*, *31*(10), 861-864.

Yang, S., F. Zhang, and Z. Wang (2012), Grain size distribution and age population of detrital zircons from the Changjiang (Yangtze) River system, China, *Chem. Geol.*, *296-297*, 26-38.

Yin, A., C. S. Dubey, T. K. Kelty, A. A. G. Webb, T. M. Harrison, C. Y. Chou, et al. (2010), Geologic correlation of the Himalayan orogen and Indian craton: Part 2. Structural geology, geochronology, and tectonic evolution of the Eastern Himalaya, *GSA Bulletin*, *122*(3-4), 360-395, 10.1130/B26461.1.

Zeilinger, G., J. P. Burg, U. Schaltegger, and D. Seward (2001), New U/Pb and fission track ages and their implication for the tectonic history of the lower Kohistan Arc Complex, northern Pakistan, *J. Asian Earth Sci.*, *19*(3S), 79-81.

Zeitler, P. K., and C. P. Chamberlain (1991), Petrogenetic and Tectonic Significance of Young Leukogranites from the Northwestern Himalaya, Pakistan, *Tectonics*, *10*(4), 729-741.

Zeitler, P. K., C. P. Chamberlain, and H. A. Smith (1993), Synchronous Anatexis, Metamorphism, and Rapid Denudation at Nanga-Parbat (Pakistan Himalaya), *Geology*, *21*(4), 347-350.

Zeitler, P. K., J. F. Sutter, I. S. Williams, R. E. Zartman, and R. A. K. Tahirkheli (1989), Geochronology and temperature history of the Nanga Parbat-Haramosh Massif, Pakistan, in *Tectonics of the western Himalayas*, edited by L. L. Malinconico and R. J. Lillie, pp. 1–22, Geological Society of America, Boulder, CO.

Zhou, P., A. Carter, Y. Li, and P. D. Clift (2019), Slowing Rates of Regional Exhumation in the Western Himalaya: Fission Track Evidence from the Indus Fan, *Geol. Mag.*, doi:10.1017/S001675681900092X.

Zhuang, G., Y. Najman, S. Guillot, M. Roddaz, P.-O. Antoine, G. Métaise, et al. (2015), Constraints on the collision and the pre-collision tectonic configuration between India and Asia from detrital geochronology, thermochronology, and geochemistry studies in the

lower Indus basin, Pakistan, *Earth Planet. Sci. Letts.*, *432*, 363–373, doi:10.1016/j.epsl.2015.10.026.

Zhuang, G., Y. Najman, Y. Tian, A. Carter, L. Gemignani, J. Wijbrans, et al. (2018), Insights into the evolution of the Hindu Kush-Kohistan-Karakoram from modern river sand detrital geo- and thermochronological studies, *J. Geol. Soc.*, doi:10.1144/jgs2018-007.

Figure Captions

Figure 1. A) Shaded bathymetric and topographic map of the Arabian Sea and surrounding area showing the location of the drilling sites considered by this study. Map also shows the major tributary systems of the Indus River, as well as smaller peninsular India rivers and their source mountains. B) Inset map shows detail of the Laxmi Basin and location of the drill sites considered in this study. Numbered red circles indicate existing scientific boreholes from Deep Sea Drilling Project (DSDP) and Ocean Drilling Program (ODP). KK = Karakoram; NP = Nanga Parbat. C) Geological map of the western Himalaya showing the major tectonic units that are eroded by the Indus River and its tributaries. Map is modified after Garzanti *et al.* [2005]. Rivers as shown in thick black lines. ISZ = Indus Suture Zone, MCT = Main Central Thrust, MBT = Main Boundary Thrust and MFT = Main Frontal Thrust. Thick black line shows the boundary of the Indus drainage, while thinner lines demark the limits of the major Himalayan tributaries. Figure is modified from Clift *et al.* [2019b].

Figure 2. Simplified lithologic logs of the two drill sites considered in this study. Black arrows show the location of the samples analyzed. Modified from Pandey *et al.* [2016c]. Pale shaded intervals show inferred lithologies based on small amounts of recovered core. Because induration is progressive and there is no sharp division, we make no attempt to distinguish between sediments and indurated rocks. Numerical ages are from Pandey *et al.* [2016a] for Site U1456 and from Pandey *et al.* [2016b] for Site U1457, with updates from Routledge *et al.* [2019].

Figure 3. Grainsize range of all samples analyzed for U-Pb zircon dating from the Laxmi Basin shown on the scheme of Folk [1974]. Samples are marked to show those published by Clift *et al.* [2019b], rather than presented new here (Table 2). Note the dominance of silty sand and sandy silt in the analyzed samples.

Figure 4. Detailed grain size spectra showing the range of sizes of the different samples considered within this study. Most of the sediment is fine sand to coarse silt in size and typically shows a coarse-skewed. A) Samples younger than 7 Ma, b) samples older than 7 Ma. Samples are marked to show those published by Clift *et al.* [2019b](gray text labels and white ringed symbol), rather than presented new here (Table 2) (black text labels and black ringed symbol).

Figure 5. (A) Geochemical signature of the analyzed samples illustrated by a CN-A-K ternary diagram [Fedo *et al.*, 1995]. CN denotes the mole weight of Na_2O and CaO* (CaO* represent the CaO associated with silicate, excluding all the carbonate). A and K indicate the content of Al_2O_3 and K_2O respectively. Samples closer to A are rich in kaolinite, chlorite and/or gibbsite (representing by kao, chl and gib). CIA values are also calculated and shown on the left side,

with its values are correlated with the CN-A-K. Samples from the delta have the lowest values of CIA and indicates high contents of CaO and Na_2O and plagioclase. Abbreviations: sm (smectite), pl (plagioclase), ksp (K-feldspar), il (illite), m (muscovite). B) Geochemical classification of sediments from this study as well as those from the Indus delta [*Clift et al.*, 2010], Indus Canyon [Li *et al.*, 2018] and western Indian shelf [Kurian *et al.*, 2013] following the scheme of Herron [1988].

Figure 6. Cross plot of Zr concentration against median sample grain size. No strong correlation is observed.

Figure 7. Kernal density estimate (KDE) diagram showing the range of the zircon U-Pb ages for individual sand grains back to 3000 Ma. Colored strips show the range of populations with diagnostic links to critical source terrains in the headwaters of the Indus. Data from the Siwaliks, as well as the Tethyan, Greater and Lesser Himalaya are compiled from DeCelles *et al.* [2004]. Karakoram data is from is from Le Fort *et al.* [1983], Parrish and Tirrul [1989], Schärer *et al.* [1990], Fraser *et al.* [2001] and Ravikant *et al.* [2009]. Nanga Parbat data is from Zeitler and Chamberlain [1991] and Zeitler *et al.* [1993]. Transhimalayan data is from Honegger *et al.* [1982], Schärer *et al.* [1984], Krol *et al.* [1996], Weinberg and Dunlap [2000], Zeilinger *et al.* [2001], Dunlap and Wysoczanski [2002], Singh *et al.* [2007], and Ravikant *et al.* [2009]. Samples are marked to show those published by Clift *et al.* [2019b], and those presented new here.

Figure 8. Kernal density estimate (KDE) diagram showing the range of the zircon U-Pb ages for individual sand grains back to 200 Ma. Colored strips show the range of populations with diagnostic links to critical source terrains in the headwaters. See Figure 6 caption for data sources.

Figure 9. Upper continental crust normalized compositions of the sediments whose zircons are the focus of the study. Bulk settlement compositions are normalized according to the average of the continental crust from Taylor and McLennan [1995].

Figure 10. Plots of relative abundance of provenance sensitive zircon age populations in individual samples compared with sample median grain size. The coarsest samples show preference for the oldest U-Pb ages and a relative lack of the younger populations.

Figure 11. Multidimensional scalar (MDS) diagrams made from zircon U-Pb age data showing (A) how the different sediment samples from IODP Expedition 355 compare with one another and post-glacial sediments from the Indus delta (TH-10-8 and KB-40-4) and (B) with the major source terranes in the Indus catchment, as well as the modern rivers of the Indus catchment, i.e., the main or trunk stream of the Indus, upstream of Attock, and its major eastern tributaries. Solid lines join sediments to their most similar neighbor, while dashed lines join the next most similar. Sources of bedrock age data come from the literature, as described in Figure 6. River data is from Alizai *et al.* [2011]. Note that sediments older than 5 Ma plot towards the right in Figure 10B, in the direction of Karakoram bedrock sources, whereas there is a progressive migration towards the left, towards Himalayan sources after that time. Diagram was constructed using the statistical package of Vermeesch *et al.* [2016].

Figure 12. Pie diagrams showing the predicted source compositions of the zircon populations in sands from the Laxmi Basin as unmixed using the software of Sundell and Saylor [2017]. Note the significant reduction in flux from the Karakoram starting ~5.72 and again at 3.02 Ma. Samples are marked to show those published by Clift *et al.* [2019b], and those presented new here.

Figure 13. Comparison of climate, erosion and exhumation proxies in the Himalaya. (a) Smoothed Nd isotope history for the Indus River with grey background showing effective uncertainties from Clift *et al.* [2018]. (b) Breakdown of the sources of detrital zircons based on the unmixing procedure of Sundell and Saylor [2017]. (c) Carbon isotope character of pedogenic carbonate in Pakistan as an indicator of dominant vegetation in the Potwar Plateau of Pakistan [Quade *et al.*, 1989], and NW India [*Singh et al.*, 2011]. (d) Relative exhumation rates of the Greater Himalaya tracked by bedrock Ar-Ar dating [*Clift et al.*, 2008b] and zircon fission track from foreland basin sediment [Chirouze *et al.*, 2015]. (e) Rates of sediment supply to the Arabian Sea calculated from regional seismic [*Clift*, 2006].

Table Captions

Table 1. Major elements major elements geochemical analysis of the samples considered in this study.

Table 2. Analytical results from the laser particle size analyzer for all bulk samples considered in this study.

Table 3. Analytical data for the zircon U-Pb dating of grains presented in this work.

Table 4. Results of the mixing modelling performed by the DZMix software of Sundell and Saylor [2017] on the detrital samples from the Laxmi Basin.